PL-TR-92-2171

AD-A282 040

STUDIES OF REGIONAL BODY AND SURFACE WAVES IN EASTERN ASIA - DATA ANALYSIS AND MODELING

Francis T. Wu
Jeffrey S. Barker

Department of Geological Sciences
State University of New York
Binghamton, NY 13902-6000

28 June 1992

Scientific Report No. 1

APPROVED FOR PUBLIC RELEASE, DISTRIBUTION UNLIMITED.

PHILLIPS LABORATORY
Directorate of Geophysics
AIR FORCE MATERIEL COMMAND
HANSCOM AIR FORCE BASE, MA 01731-3010

The views and conclusions contained in this document are those of the authors and should not be interpreted as representing the official policies, either expressed or implied, of the Air Force or the U.S. Government.

This technical report has been reviewed and is approved for publication.

JAMES F. LEWKOWICZ
Contract Manager
Solid Earth Geophysics Branch
Earth Sciences Division

JAMES F. LEWKOWICZ
Branch Chief
Solid Earth Geophysics Branch
Earth Sciences Division

DONALD H. ECKHARDT, Director
Earth Sciences Division

This document has been reviewed by the ESD Public Affairs Office (PA) and is releasable to the National Technical Information Service (NTIS).

Qualified requestors may obtain additional copies from the Defense Technical Information Center. All others should apply to the National Technical Information Service.

If your address has changed, or if you wish to be removed from the mailing list, or if the addressee is no longer employed by your organization, please notify PL/IMA, Hanscom AFB MA 01731-5000. This will assist us in maintaining a current mailing list.

Do not return copies of this report unless contractual obligations or notices on a specific document requires that it be returned.

REPORT DOCUMENTATION PAGE

Form Approved
OMB No 0704-0188

1. AGENCY USE ONLY (Leave blank)	2. REPORT DATE	3. REPORT TYPE AND DATES COVERED
	28 June 1992	Scientific No. 1

4. TITLE AND SUBTITLE
Studies of Regional Body and Surface Waves in Eastern Asia
- Data Analysis and Modeling

5. FUNDING NUMBERS
PE 62101F
PR 7600 TA 09 WU AR
Contract F19628-90-K-0042

6. AUTHOR(S)
Francis T. Wu
Jeffrey S. Barker

7. PERFORMING ORGANIZATION NAME(S) AND ADDRESS(ES)
Department of Geological Sciences
State University of New York
Binghamton, NY 13902-6000

8. PERFORMING ORGANIZATION REPORT NUMBER

9. SPONSORING/MONITORING AGENCY NAME(S) AND ADDRESS(ES)
Phillips Laboratory
29 Randolph Road
Hanscom AFB, MA 01731-3010

Contract Manager: James Lewkowicz/GPEH

10. SPONSORING/MONITORING AGENCY REPORT NUMBER
PL-TR-92-2171

11. SUPPLEMENTARY NOTES

12a. DISTRIBUTION AVAILABILITY STATEMENT
Approved for public release;
distribution unlimited

12b. DISTRIBUTION CODE

13. ABSTRACT *(Maximum 200 words)*

This report consists of two parts. The first consists of a surface wave regionalization and tomographic analysis of China. The second involves modeling of regional body waveforms from earthquakes in western China.

Love and Rayleigh waves recorded at CDSN stations for earthquakes within China and on its periphery are used to determine dispersion along more than 400 paths in China and its immediate vicinity. These data are used to determine the dispersion characteristics of 17 regions, which may then be inverted for velocity structure. We have also attemptied to determine the anisotropic nature of the crust and and upper mantle of this area. However, at present, the data is not sufficient to resolve the additonal parameters.

Regional body waves have been collected and modeled from a profile of earthquakes located southwest of CDSN station WMQ. The profile is compared to a profile of synthetic seismograms computed using a frequency-wavenumber integration technique with an assumed velocity structure model. Since the depths of the different earthquakes varies, we also compare individual P waveforms with synthetics computed for 10, 20 and 30 km depth. The variable moveout of different phases within the P_n-P_g wavetrain enables a fairly accurate determination of source depth. This illustrates that the interference of phases that contribute to the regional P_n-P_g waveforms can serve as a discriminant.

14. SUBJECT TERMS	15. NUMBER OF PAGES
Regional surface waves, regional body waves, China	54
	16. PRICE CODE

17. SECURITY CLASSIFICATION OF REPORT	18. SECURITY CLASSIFICATION OF THIS PAGE	19. SECURITY CLASSIFICATION OF ABSTRACT	20. LIMITATION OF ABSTRACT
Unclassified	Unclassified	Unclassified	SAR

Surface Wave Regionalization and Tomography in China and its Vicinity

Francis Wu and Alan Jones
State University of New York, Binghamton

Introduction

In the broadest outline, Continental China and its immediate vicinity can be represented as a mosaic of blocks that were accreted through geological ages. In general, Siberian shield can be considered the core, with generally younger terrains appended to it at later times. Much of the insight on the continental tectonics of that area is gained from surface geological observation (Yang, 1986). The deeper seismic strucutres of this area remain relatively unknown. Judging from a limited number of crustal profiles that had been shot and few surface wave studies in China, the crust in this area is laterally very heterogeneous. Several surface wave dispersion studies have been done outside of China by using data recorded at stations on the periphery; the foci of these studies are often concentrated on Tibet, one of the outstanding tectonic features of this area. As a result of the establishment of high quality seismic stations in China, many studies are now possible. It is still a very sparse network in that station spacing in on the order of 1000 km. For surface waves however, it is quite sufficient.

In this report, surface waves recorded at the Chinese Digital Seismic Network (CDSN) stations from earthquakes within the area are used to determine the group velocities of both Rayleigh and Love waves along more than two hundred paths. We then employ these dispersion curves in two studies. By adopting a regionalization scheme based on the geological map of China, we can determine the "pure path" dispersion characteristics of these regions and and determine the velocity model for these regions. We can also avoid making a priori assumptions of regions and construct a tomographic image of the area. The two methods are complementary in that the tomographic

result provides an overall picture of the structural variations in the area and thus give an independent assessment of the soundness of the regionalization scheme. On the other hand, to invert for velocity structure, the construction of a dispersion curve from the tomographic image is not a straightforward task as the result is smoothed differently at each period; the regionalization result is readily invertible.

Of the previous surface wave studies in this area, most of them are done with data external to the region of interest. Chun and Yoshii (1977) used events on the eastern side of the plateau and stations south of the Himalayas; they aim they study at Tibet. Patton (1980) and Feng and Teng (1983) studied a large portion of Eurasia with Rayleigh waves traversing through the area; while Patton (1980) defined the regions based on topography and known crustal thicknesses, Feng and Teng (1983) divided the region into 10° x 10° grid. Brandon and Romanowicz (1986) employ the "two-event" technique to determine dispersion curves in northern Tibet. Feng et al. (1983) used data recorded on Kirnos seismographs from stations within China to derive surface wave dispersion in the period range of 10 to 50 seconds. Relatively few paths were used in their study. Some paths are within the tectonic units Feng et al. (1883) determined; for paths that covered more than one region the fractional path composition is assigned and the dispersion in the desired region extracted.

Although the the amount of surface data recorded within east Asia is increasing rapidly, with the establishment of CDSN and later stations in the Russian and other republics, as far as the regionalization study is concerned, the need to achieve a balance between the data available and the details to be resolved remains. We started our study with more than 31 regions, representing reasonably well the main features shown in the 1:4,000,000 Geology Map of China (Ministry of Geology, 1976). Among the 31 regions, some have areas less than 50,000 km^2 and are ill resolved in the inverersion. Subsequent tests involving the monitoring of model resolution and statistical significance with reduced number of blocks, with the desire that most of the distinct tectonic blocks be included and significantly resolved. The statistical measures used to assess the statistical significance of the result are the Akaike Final Prediction Error (FPE; Akaike, 1969) and the F-test (Jacobson and Shaw, 1991); the results of these tests corroborate each other, giving us confidence

in the results. In view of the importance of anisotropy in the study of crust and upper mantle, we have also subjected our data to such analyses. The anisotropic parameters thus obtained however, are found not to be statistically significant.

In our tomographic inversion a modified Gilbert-Backus method (Ditmar and Yanovskaya, 1987; Keilis-Borok et al., 1989) is employed. This method has the advantage that it does not require a subjective choice of boundaries; instead, for each period, it produces a smooth group velocity distribution of the area covered by the raypaths, with its resolution (in km) depending on the distribution of paths.

The tomographic images of the region as a whole and the velocity structures obtained from inversion of Rayleigh and Love wave dispersion curves for various tectonic regions show clearly the lateral variations in crustal structures. Tibet is by far the most prominent features in the region, but we are able to resolve smaller features as well. Only very preliminary results are shown here. Further work will be published in a paper under preparation (Wu, Levshin and Jones, 1992).

Data

Figure 1 shows the location of the 69 events and the CDSN stations; the event data are also listed in Table I. Because of the wide dynamic range of the CDSN seismic system, although the records stay on scale for magnitude 7 earthquakes, surface waves from $M_S \sim = 4.3$ can be used to determine group velocities in the 20-70 second range. The 69 events used in this study are located within and around the study area (Table II and Figure 1), yielding altogether more than 200 Love and Rayleigh dispersion curves. The group velocity dispersion curves are determined with an interactive multiple filter group velocity program on workstations, allowing rapid group velocity determination and visual quality control. Table II presents a list of events used in this study.

Methodology

Regionalization

Isotropic model

Assuming that a surface wave passes through various tectonic blocks and the velocities vary in each block. We can write, for the kth path (between an epicenter and a station) at one frequency as:

$$\frac{1}{U_k} = \sum_{i=1}^{i=n} \frac{\Delta_{ik}}{U_i} \tag{1}$$

$\frac{1}{U_k}$ is the group slowness, Δ_{ik} is the length of path in the ith block, and U_i is the group velocity in the ith block that we wish to find. Let us write this system of equations as:

$$Ds = t \tag{2}$$

where D is the matrix formed from the lengths of paths in each region, s is the vector of slownesses to be determined and t is the vector of measured group slowness for each path. This over-determined set of equations is solved in a least-squared sense using the method of Singular Value Decomposition (SVD; see for example, Press et al., 1985). The solution is repeated for each period.

Anisotropic model

In our study we use the same formulation as that of Nishimura and Forsythe (1988), in which azimuthal anisotropy is determined. A set of equations including the anisotropic parameters can be written in the same form as (2). And SVD can again be employed for its solution.

Resolution and statistical assessment

Once the solution of equations (2) is found, one can compute the summed-squared residual of the errors:

$$SSR = \Sigma(t - t')^2 \tag{3}$$

where t is the measured travel time and t' is the predicted travel time.

If all of the eigenvectors obtained from the SVD procedure are used, the solution will have large variances due to the presence of small eigenvalues. The usual practice is to discard the smallest eigenvalues which has the effect of discarding some of the eigenvectors. As more eigenvalues are retained, the SSR becomes smaller.

One method to determine how many eigenvalues should be retained is the sequential F-test (Jacobson and Shaw, 1991). To use the F-test, one computes the SSR for the case of one retained eigenvalue. Then additional eigenvalues are added one at a time. The F-test is applied using the SSR compared with the SSR obtained with just one eigenvalue. When it is determined that there is a significant difference between the SSRs at some level (e.g. 95%), then these eigenvalues are retained. More eigenvalues are again added one by one and compared with the last significant SSR. The F statistic is computed as:

$$F = \frac{((SSR_k - SSR_p)/(p - k))}{(SSR_p/(n - p))} \tag{4}$$

where p is the number of eigenvalues retained, k is the previous number retained which gave a significant result and n is the number of equations. It should be pointed out that the F-test is only valid if the errors have a gaussian distribution.

Another method to determine the number of eigenvalues to keep is due to Akaike (1969). Akaike computes a Final Prediction Error (FPE):

$$FPE = SSR_p \frac{(1 + p/n)}{(n - p)} \tag{5}$$

where p is the number of retained eigenvalues and n is the total number of eigenvalues. The number of eigenvalues to retain is given by the value of p which yields the smallest FPE.

Tomography

The method used in this study is described in detail in Keilis-Borok (1989).

The first step involves the transformation of spherical coordinates θ, ϕ to that of x, y. The transformation

$$x = R_0 \ln \tan(\theta/2)$$

$$y = R_0 \phi \tag{6}$$

$$V(x, y) = v(\theta, \phi)/\sin\theta$$

where R_0 is the Earth's radius. The distortion of $v(\theta, \phi)$ is minimized in this transformation if $\sin\theta$ does not vary too much within the area. By transforming the area to that around two sides of the equator reduces the error. One gains maximum advantage if the new equator lies along the long diagonal of a roughly rectangular area.

The travel time between two points (x_{0j}, y_{0j}) and (x_{1j}, y_{1j}) can be represented as

$$t_j = \int_{(x_{1j}, y_{1j})}^{(x_{0j}, y_{0j})} V^{-1}(x, y) ds \tag{7}$$

We wish to solve $V^{-1}(x, y)$ under smoothing and other constraints.

Regionalized Dispersion of China and Results of Inversion

The basis for regionalization

In our preliminary work (Wu, 1989), we have tested a detailed regionalization scheme that including a total of 31 regions in China and its vicinity. The boundaries follow closely those in the geology map of China. As it was shown in Wu (1989) the resolution for many regions were quite poor. We group regions with similar tectonics, judged on the basis on types of rocks, platformal, with Bouguer gravity anomaly, and other crustal studies, our general tectonic understanding, as well as the ray paths coverage, which determines the resolvability of the regions, we have divided China and its vicinity into seventeen regions. We have kept the regions that were resolved in the earlier study (Wu, 1989), and combined those that are tectonically similar (in age, lithology or gravitational characteristics). The boundaries of these blocks are shown in Figure 1. The ray paths coverage is shown in Figure 2.

Results

The final regionalization scheme we have adopted allows us to look at the dispersion characteristics of the main tectonic provinces of China and its vicinity.

Dispersion curves

Figure 3 shows the Rayleigh dispersion curves of the seventeen regions marked in Figure 1, and Figure 4 shows the corresponding curves for Love waves. Although the results for some of the regions remain unchanged from those presented in Wu (1989), the new regionalization lessens the trade-offs in the resolution matrix (Figure 5 and 6). These curves are now being inverted for velocity structures.

F-Test and FPE test

The F-test and FPE tests described earlier were used in the SVD inversion for regionalized dispersion curves. As shown in Figures 7 and 8, the minima for F-test and FPE coincide, N=15,

for both Rayleigh and Love waves, and accordingly, 15 eigenvalues were retained in the solution for group velocity. The minima are quite subtle but can be determined by examining the numbers which generated these plots.

Anisotropic Crust and Upper Mantle?

Anisotropy determination based on shear wave splitting has been found to be indicative of regional stress directions. Nishimura and Forsyth (1988) has used regionalized data in the Pacific Ocean for the determination of anisotropy related to ocean floor spreading. In this study we use formulation identical to that of Nishimura and Forsyth in an attempt to see whether we can resolve the anisotropy using our data. We then use the F-test and FPE to determine how many eigenvalues can be retained. For this test, we concoct a model with only seven regions as shown in Figure 9. There are altogether 21 parameters to be resolved.

Results

Figure 10 shows the Love wave dispersion curves for the seven regions. The solid line in each frame represents the isotropic results and the two dashed lines show the fast dispersion (above the solid line) and the slow dispersion (below the solid line). The anisotropic velocities are as much as 10% above or below the isotropic values.

Resolution and error estimates

When anisotropy is considered, the number of parameters is three times the number in the isotropic case. In this case the FPE and F-test both say that only one eigenvalue should be retained (Figure 11). The results shown in Figure 10 are those when all eigenvalues are retained

Tomography

In this report we shall only present partial results of what is being done in using the same dataset for tomographic studies. Figures 12 and 13 show images of Rayleigh and Love group

velocities at 50 seconds. One of the most prominent features seen in these images is the Tibetan plateau in western China. The rapid increase of group velocity east of Tibet is consistent with the high gravity gradient there, indicating is rapid change in crustal thickness in that region. The results will be presented in paper under preparation (Wu and Levshin, 1992, in preparation).

Discussion and Conclusion

Surface regionalization and tomography remain to be a powerful method in areas where a sparse, but high quality, network exists. Regionalization allows us to obtain dispersions for different tectonic areas while tomographic study provides direct images of the main velocity provinces.

References

Akaike, H., Fitting autoregressive models for prediction, Annals Inst. Statis Math., 21, 243-247, 1969.

Brandon, C. and Romanowicz, B., A "no-lid" zone in the central Chang-Thang platform of Tibet: Evidence from pure path phase velocity measurements of long period Rayleigh waves, J. Geophys. Res., **91**, 6547-6564, 1986.

Chen, W.P., and P. Molnar, Constraints on the seismic wave velocity structure beneath the Tibetan plateau and their tectonic implications, J. Geophys. Res., **86**, 5937-5962, 1981.

Chun, K. Y. and McEvilly, T. V., Crustal structure in Tibet: High seismic velocity in the lower crust, J. Geophys. Res., **91**, 10405-10411, 1986.

Chun, K. Y. and Yoshii, T., Crustal structure of the Tibetan Plateau: A surface wave study by a moving window analysis, Bull. Seismo. Soc. Am., **67**, 737-750, 1977.

Ditmar, P.G. and T. B. Yanovskaya, A generalization of the Backus-Gilbert method for estimation of lateral variations of surface wave velocity, Izv. AN SSSR, Fizika Zemli (Solid Earth), no. 6, 30-40, 1987.

Feng, R., J.S. Zhu, Y.Y. Ding, G.Y. Chen, Z.Q. He, S.B. Yang, H.N. Zhou, K.Z. Sun, Crustal structure in China from surface waves, Chinese Geophysics (AGU), **2**, 273-289, 1983.

Jacobson, R.S. & P.R. Shaw, Using the F-test for eigenvalue decomposition problems to find the statistically 'optimal' solution, Geophys. Res. Lett., 18, 1075-1078, 1991.

Feng, C. C. and Teng, T., Three-dimensional crust and upper mantle structure of the Eurasian continent, J. Geophys. Res., **88**, 2261-2272, 1983.

Keilis-Borok, V. I. (ed.), Seismic Surface Waves in a Laterally Inhomogeneous Earth, Kluwer Academic Publishers, Dordrecht/Boston/London, 1989.

Patton, H., 1980. Crustal and upper mantle structure of the Eurasian continent from the phase velocity and Q of surface waves. J. Rev. Geophys. Space Phys. 18: 605-625.

Pines, I., Teng, T., Rosenthal, R. and Alexander, S., 1980. A surface wave dispersion study of the crustal and upper mantle structure of China. J. Geophys. Res., 85: 3829-3844.

Press et al., Numerical Recipe, Cambridge University Press, 1985.

Rodi, W. L., P. Glover, T. M. C. Li, and S. S. Alexander, A fast, accurate method for computing group velocity partial derivatives for Rayleigh and Love waves, Seismo. Soc. Am., **65**, 1105-1114, 1975.

Takeuchi, and Saito, Seismic surface waves, Methods in Computational Physics, v. 11 (ed. B. Bolt), pp. 217-295, 1972.

Wu, F. T., Studies of regional phases and discriminants in Asia, *Final Report*, GL-TR-90-0017, Air Force Geophysical Laboratory, 1990. ADA222184

Yang, Z.Y., Cheng, Y. Q., and Wang, H.Z., The Geology of China, Clarenden Press, Oxford, 303pp, 1986.

Table I. List of events used in this study.

Date	Origin Time	Lat(N)	Lon(E)	D(km)	m_b	M_s	Date	Origin Time	Lat(N)	Lon(E)	D(km)	m_b	M_s
01-05-87	22:52:46.5	41.96	81.32	17.0	5.9	5.8	08-02-87	00:58:06.7	49.84	78.89	0.0	5.9	3.8
01-07-87	18:19:08.8	34.26	103.40	33.0	5.5	5.5	08-05-87	10.24:21.1	41.36	82.11	33.0	4.8	4.5
01-19-87	07:46:24.4	28.39	83.68	33.0	5.2	4.3	08-09-87	21:14:58.2	29.42	83.65	34.0	5.6	4.8
01-19-87	08:12:05.8	28.24	83.57	33.0	4.9		08-10-87	12:12:14.1	38.19	106.37	33.0	5.4	
01-24-87	08:09:21.3	41.53	79.32	29.0	5.9	5.9	09-06-87	23:38:52.2	26.69	93.37	42.0	5.1	4.3
01-24-87	08:13:14.4	41.41	79.35	33.0	5.5		09-16-87	17:57:26.7	52.11	95.66	33.0	4.8	
01-24-87	10:34:26.1	27.66	92.69	27.0	4.9		09-18-87	21:58:36.6	47.28	89.67	10.0	5.3	4.8
01-24-87	13:40:40.3	41.44	79.25	33.0	5.2		09-25-87	23:16:27.5	29.77	90.27	11.0	5.3	4.9
01-28-87	12:12:15.9	45.36	96.14	33.0	5.1		09-27-87	06:12:42.5	34.06	80.67	33.0	4.9	4.5
02-23-87	00:21:21.2	38.98	70.71	33.0	5.0	4.7	09-29-87	17:30:29.1	29.73	90.41	33.0	4.8	
02-25-87	19:56:35.5	38.10	91.18	26.0	5.7	5.7	10-03-87	11:00:03.3	36.49	71.46	80.0	6.0	
03-01-87	13:31:09.4	28.64	95.92	33.0	5.1		10-06-87	13:06:20.4	43.44	88.48	33.0	4.8	4.0
03-01-87	17:59:10.0	49.78	102.75	24.0	4.8		11-03-87	18:24:49.7	33.07	86.91	33.0	4.9	4.3
03-03-87	09:41:33.6	41.29	79.30	33.0	5.1	5.0	11-15-87	03:31:06.7	49.87	78.79	0.0	6.0	4.8
03-09-87	03:13:40.9	38.16	73.96	51.0	4.8	4.4	12-13-87	03:21:04.7	49.96	78.85	0.0	6.1	4.5
03-12-87	01:57:17.2	49.94	78.82	0.0	5.5	3.9	12-17-87	12:17:23.4	41.83	83.05	33.0	5.1	4.3
03-26-87	11:56:54.2	41.69	69.84	20.0	5.1	4.3	12-21-87	04:28:22.9	38.72	70.78	14.0	4.8	4.7
03-29-87	23:16:46.8	27.17	100.04	33.0	5.0		12-22-87	00:16:39.1	41.36	89.66	22.0	5.9	5.2
04-02-87	13:30:44.4	35.75	80.82	33.0	4.8	4.1	12-27-87	03:05:04.7	49.83	78.74	0.0	6.1	4.5
04-03-87	01:17:08.0	49.93	78.83	0.0	6.2	4.7	01-03-89	04:41:12.0	29.49	131.43	40.0	5.8	5.6
04-09-87	07:25:35.7	35.50	87.07	33.0	4.8	4.9	01-06-89	19:08:27.3	36.40	141.75	43.0	5.4	5.8
04-09-87	20:01:19.5	35.51	80.65	33.0	4.9		01-18-89	18:22:47.6	30.18	100.22	35.0	5.0	
04-17-87	01:03:04.8	49.89	78.69	0.0	6.0	4.3	01-21-89	14:06:12.2	29.51	131.51	33.0	5.4	5.5
04-30-87	05:17:37.0	39.76	74.57	8.0	5.7	5.6	01-21-89	17:37:37.5	29.51	131.47	32.0	5.2	
05-11-87	05:19:10.4	51.71	105.48	27.0	5.0	4.2	01-21-89	20:42:38.2	29.47	131.47	33.0	5.4	5.0
05-18-87	01:53:51.0	25.27	94.20	50.0	5.7	5.9	01-22-89	01:14:00.6	29.58	131.53	33.0	5.0	4.8
06-08-87	13:30:32.8	39.75	74.62	10.0	5.1	4.3	01-22-89	22:20:17.9	41.81	144.28	25.0	6.0	6.3
06-11-87	12:08:42.8	28.84	105.03	40.0	4.8		01-24-89	20:03:39.0	42.23	142.69	50.0	5.6	5.4
06-20-87	00:53:04.8	49.91	78.73	0.0	6.1	4.2	03-06-89	14:39:42.6	35.55	140.44	42.0	5.9	5.6
06-24-87	02:29:45.8	40.80	74.13	33.0	4.9	4.3	03-15-89	01:28:43.0	26.07	128.39	33.0	5.1	
06-28-87	01:16:38.2	37.68	101.60	26.0	4.9		03-20-89	02:36:50.3	24.24	125.17	29.0	5.3	5.4
07-10-87	08:17:33.6	27.36	96.89	33.0	4.8		03-30-89	14:12:12.9	41.84	143.66	23.0	5.4	5.0
07-17-87	01:17:07.0	49.78	78.13	0.0	5.8	4.6	05-13-89	03:35:02.8	50.14	105.41	33.0	5.5	5.4
07-17-87	17:23:26.9	38.97	71.02	33.0	4.8		05-15-89	18:05:36.7	24.21	122.36	33.0	5.2	

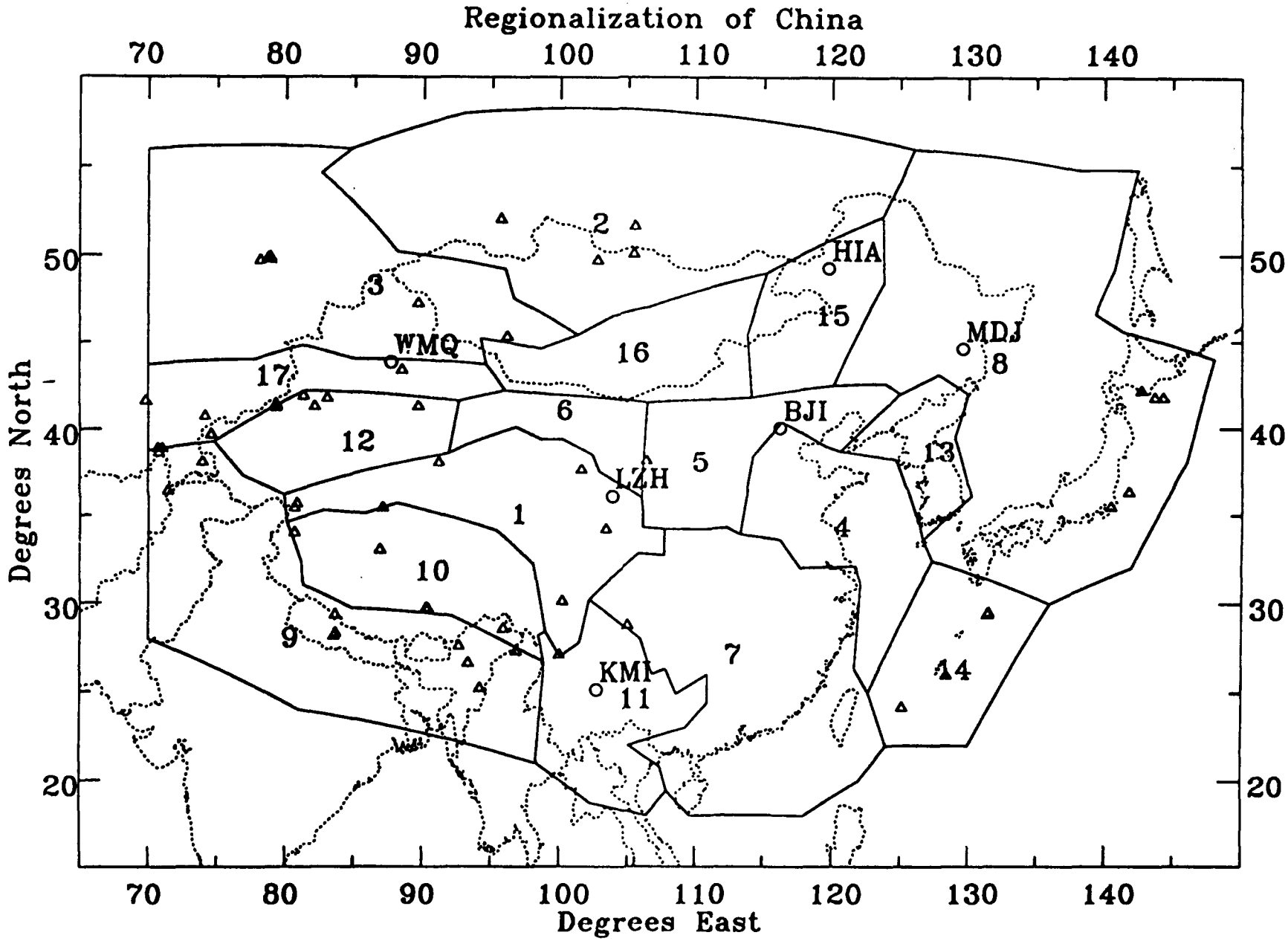

Figure 1. Locations of stations and events used in the study. The regionalization is also shown.

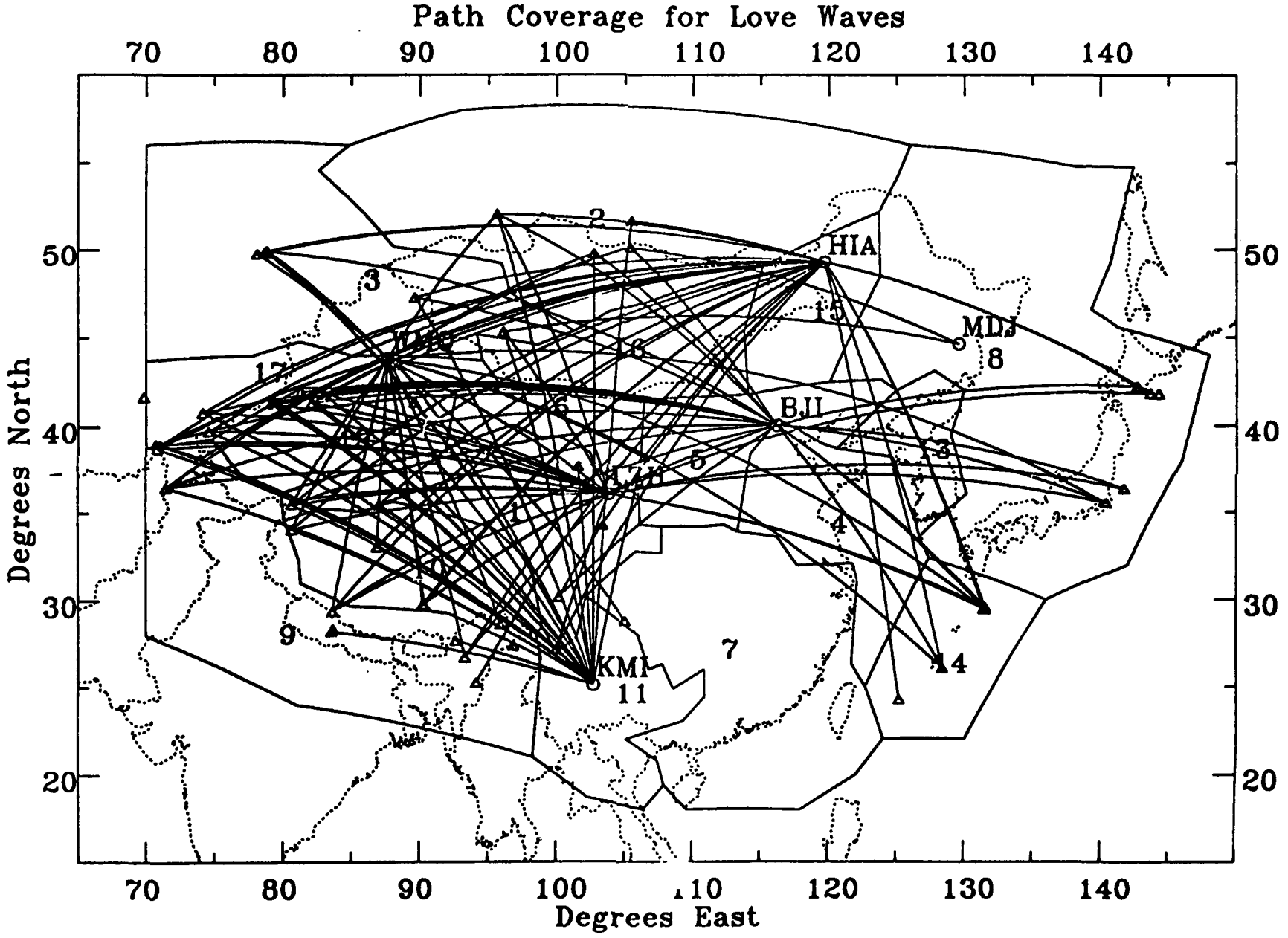

Figure 2. Ray paths for both Rayleigh and Love waves used in this study.

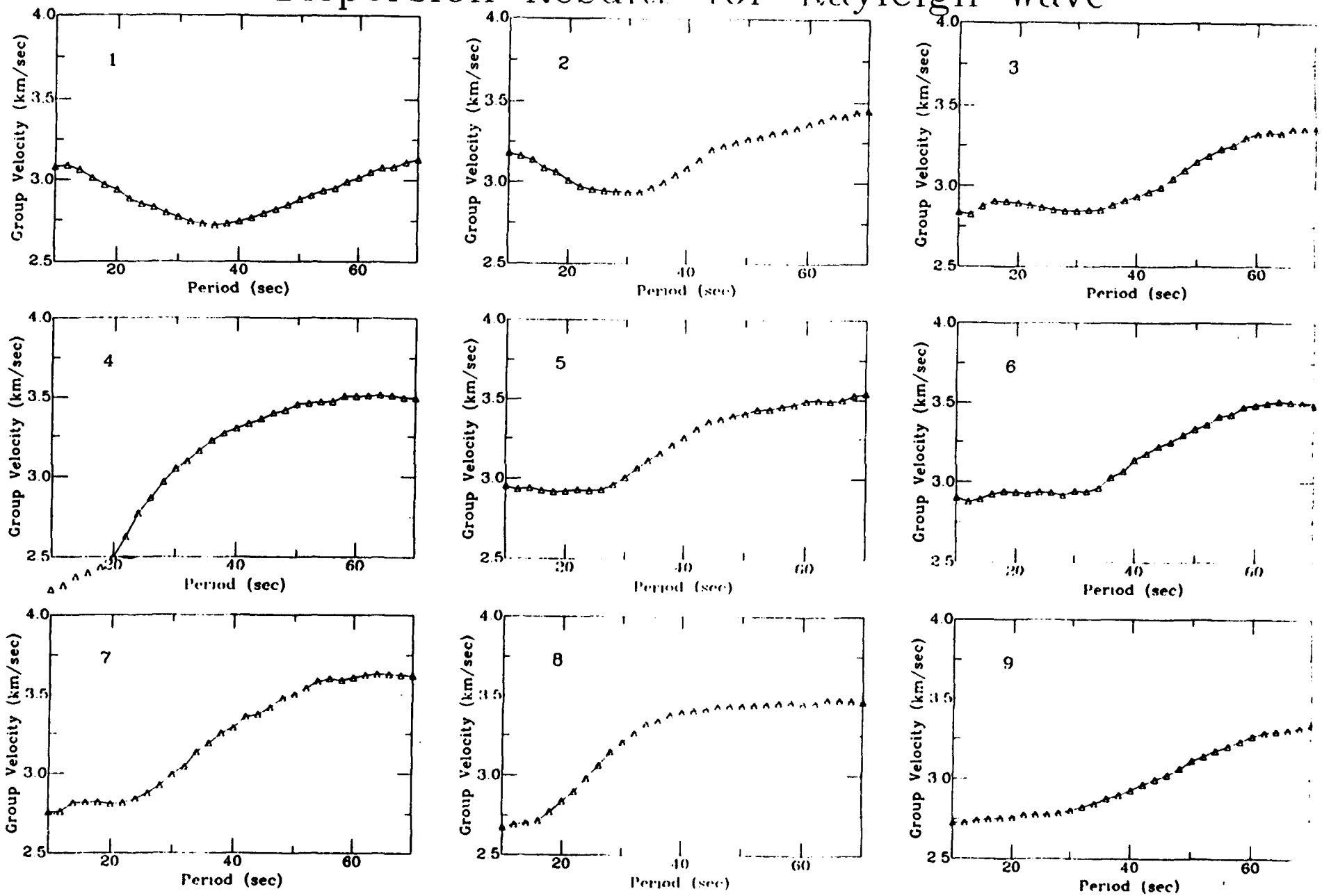

Figure 3. Rayleigh dispersion curves of the seventeen regions shown in Figure 1.

Dispersion Results for Rayleigh Wave

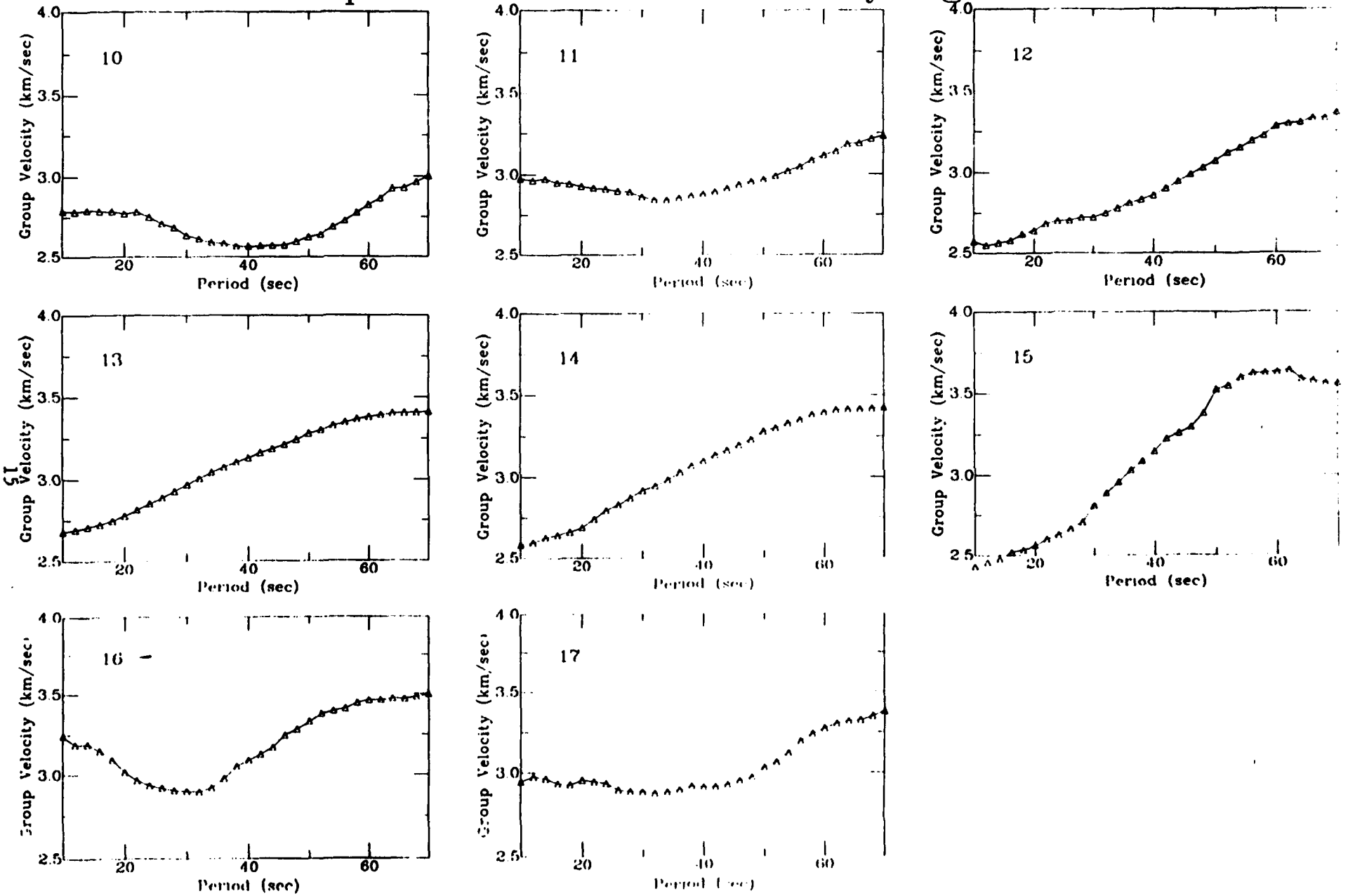

Figure 3 (continued)

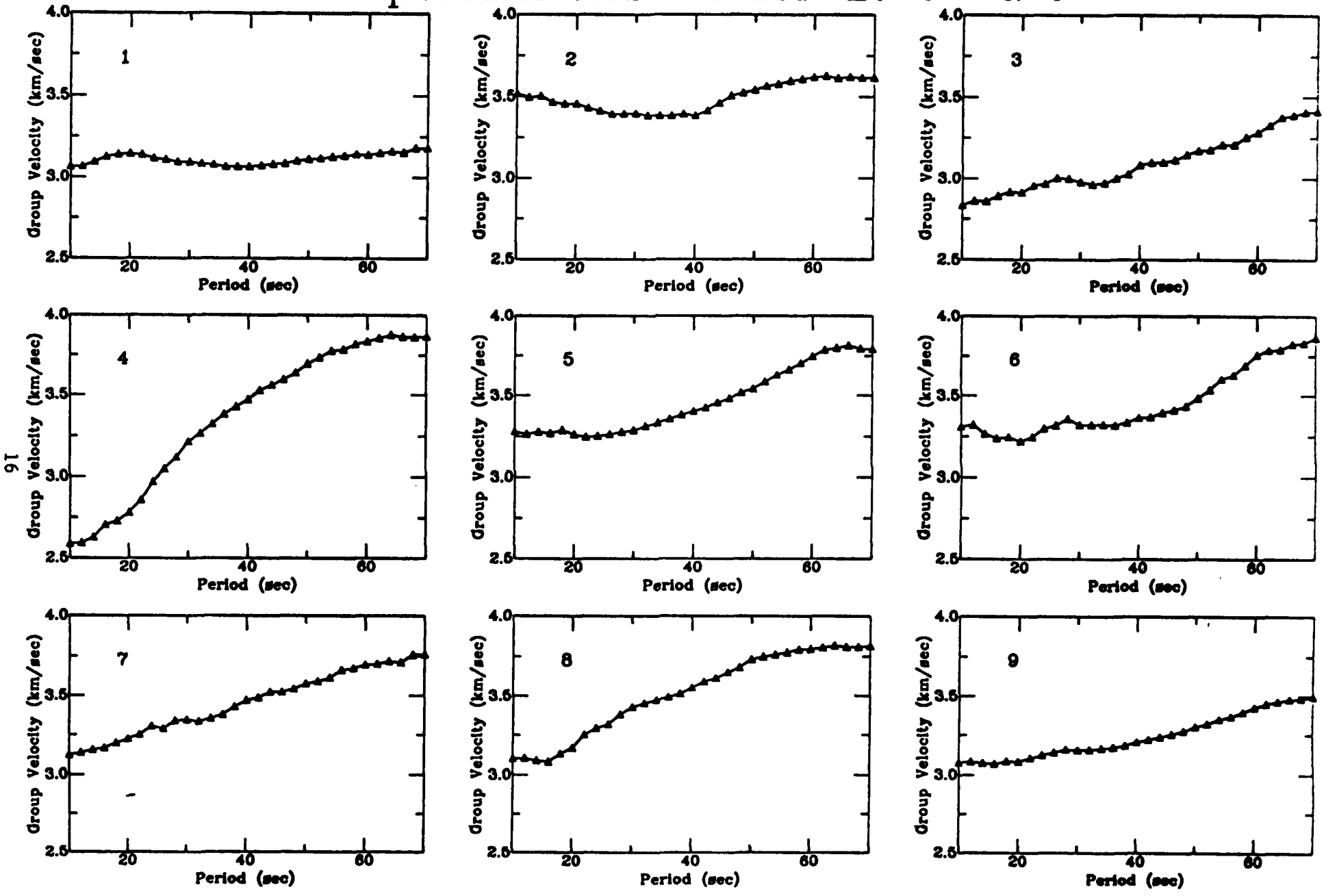

Figure 4. Love dispersion curves of the seventeen regions shown in Fig. 1.

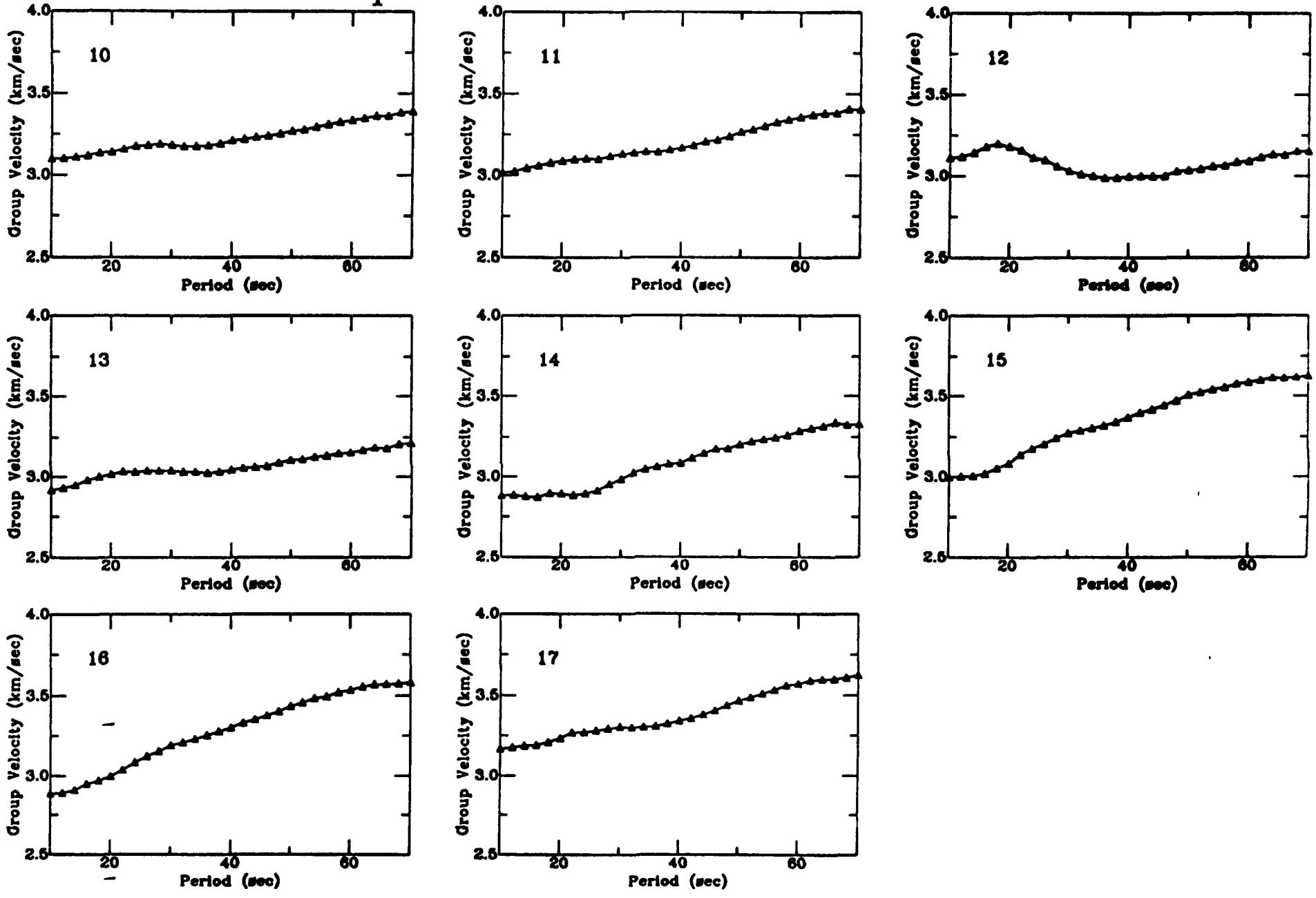

Figure 4 (continued).

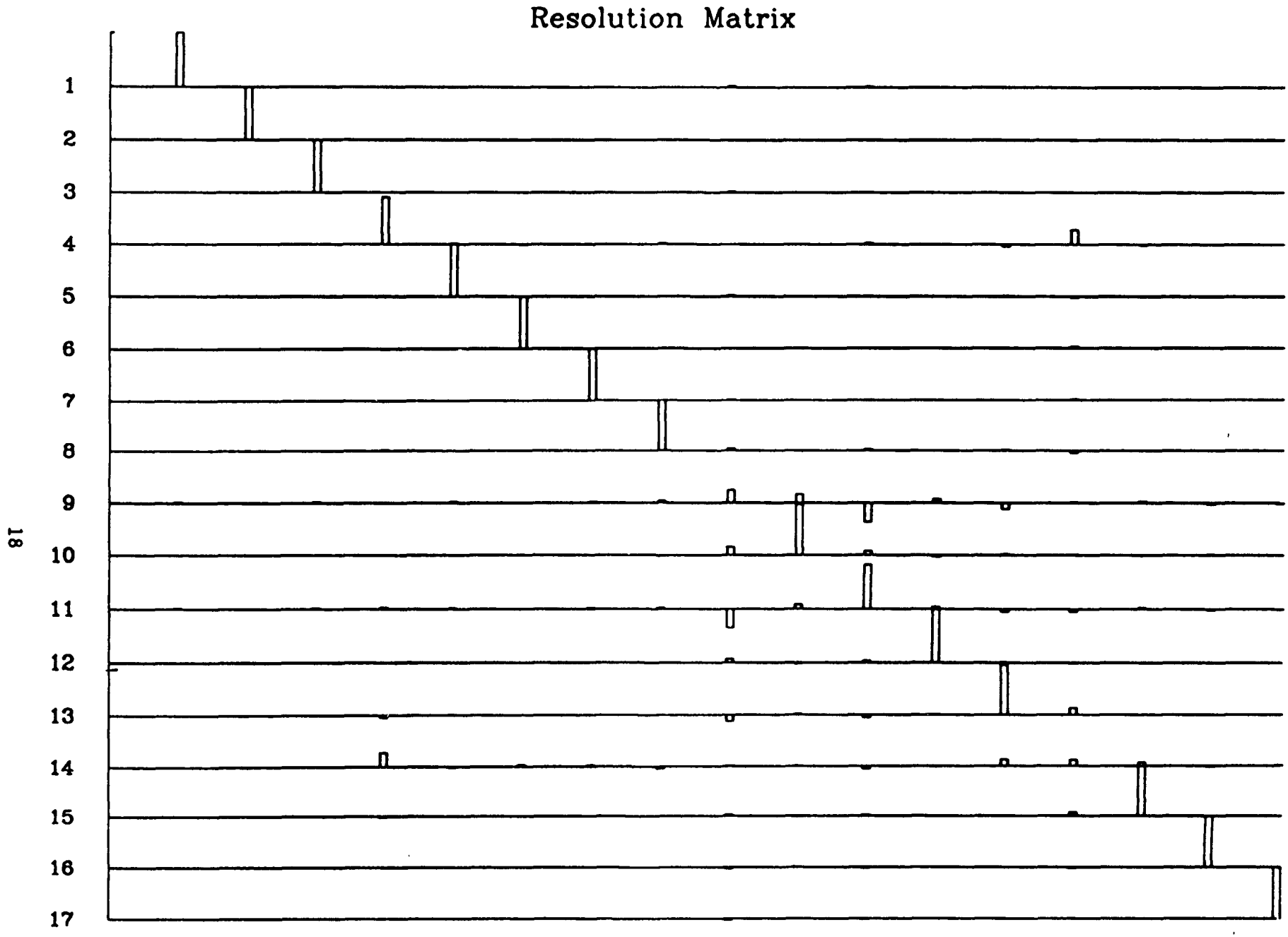

Figure 5. Resolution matrix for Rayleigh waves for the seventeen regions.

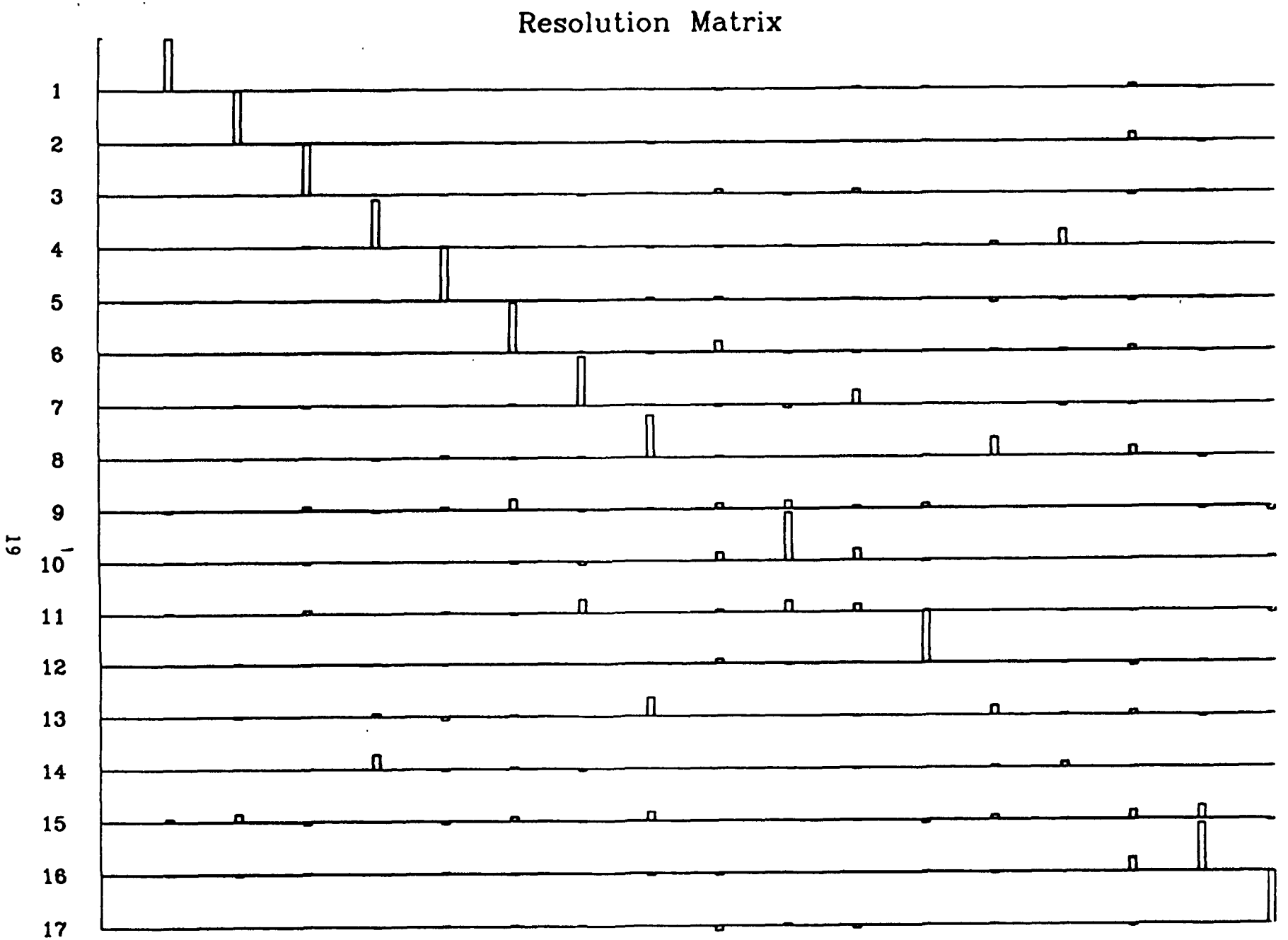

Figure 6. Resolution matrix for Love waves for the seventeen regions.

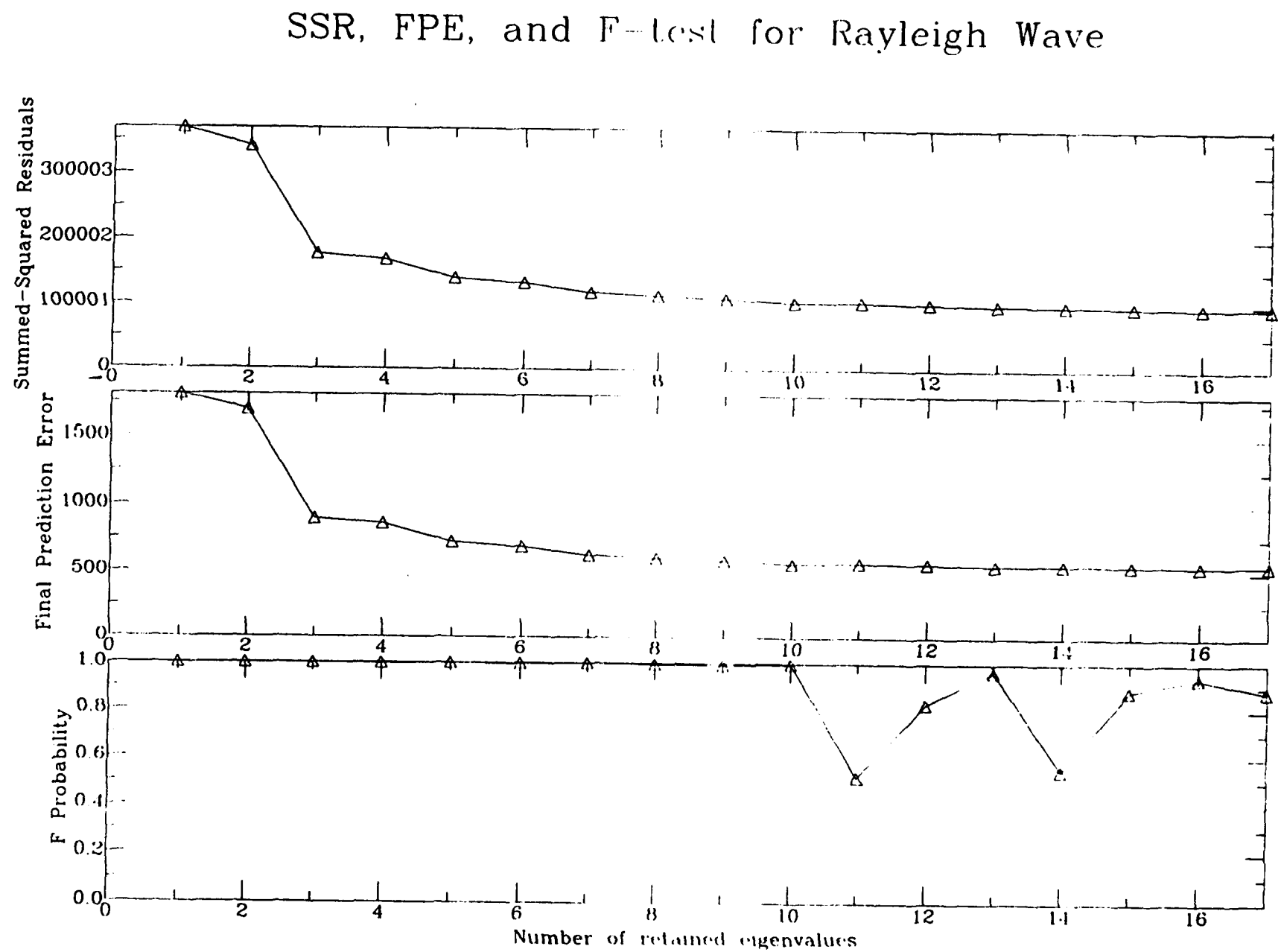

Figure 7. SSR, F-Test and FPE results for Rayleigh waves.

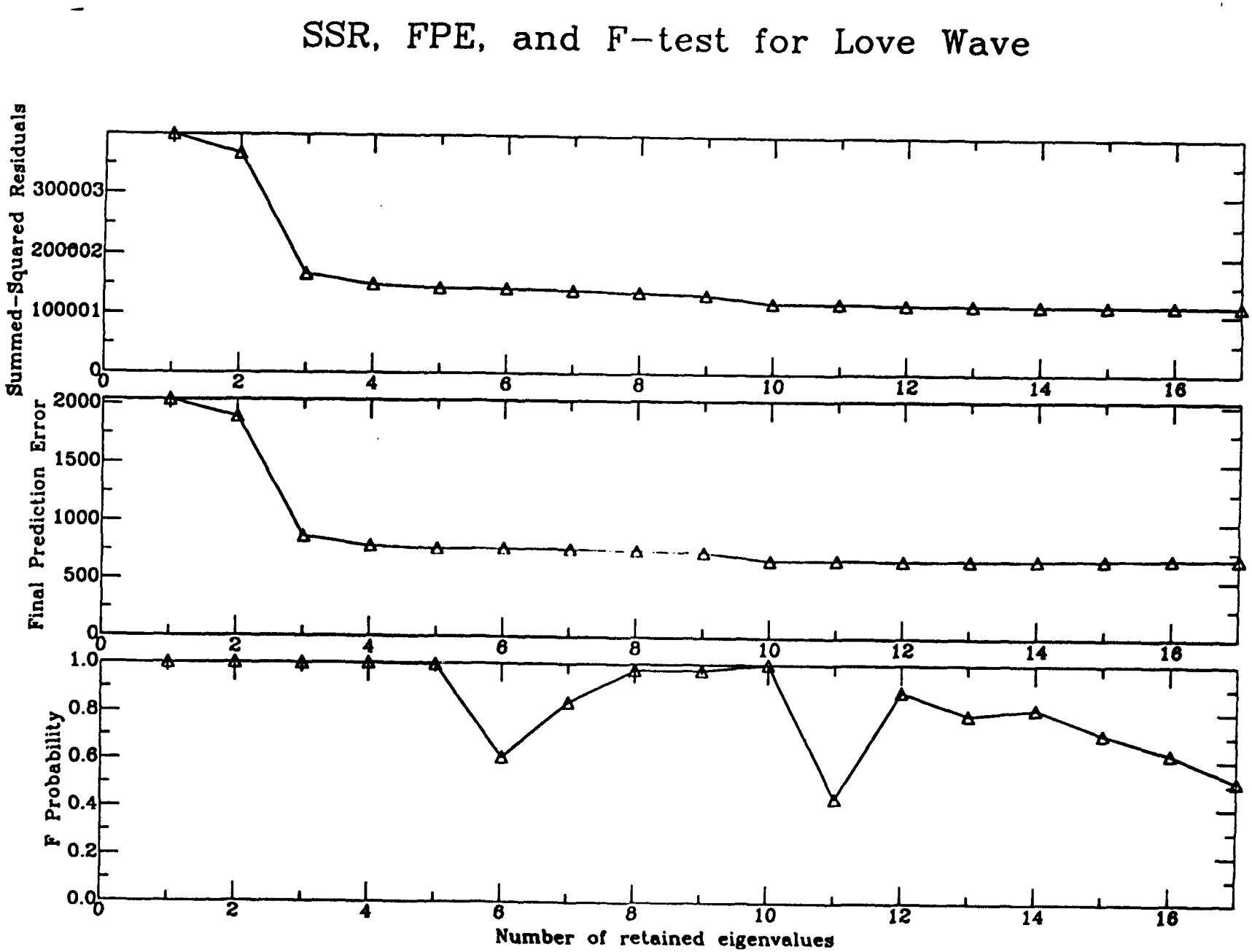

Figure 8. SSR, F-Test and FPE results for Love waves.

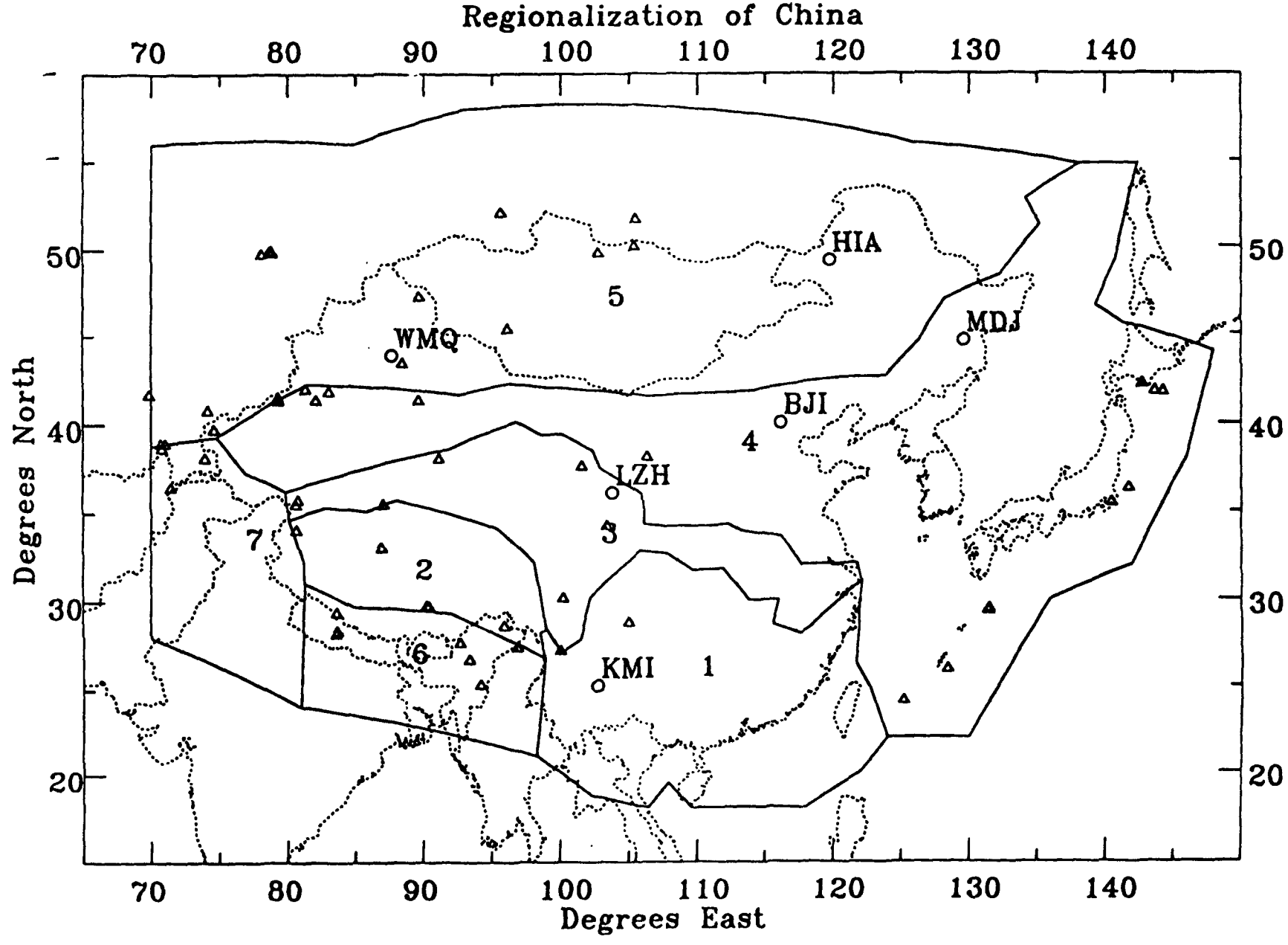

Figure 9. Regionalization with only seven regions.

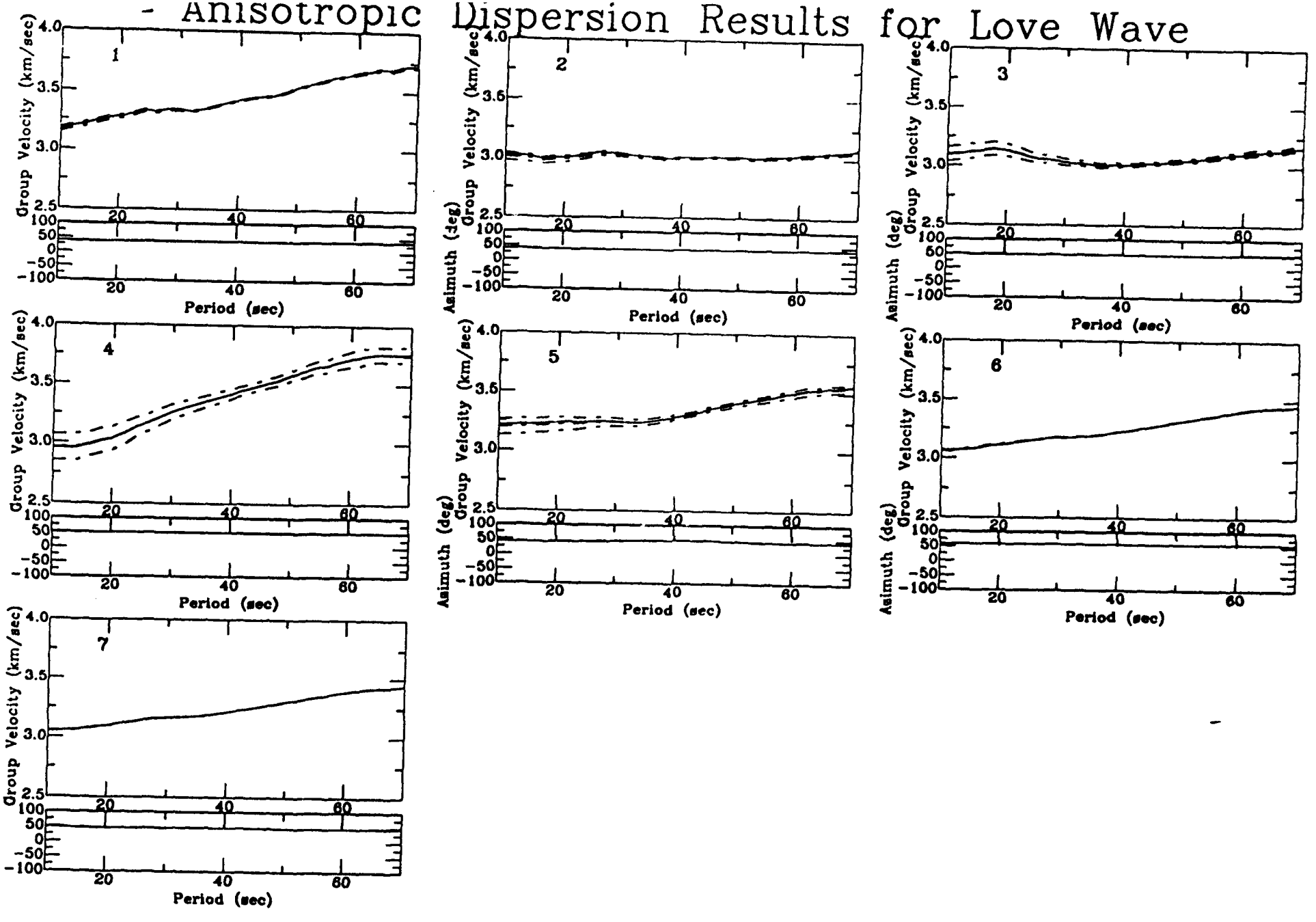

Figure 10. Anisotropic Love wave dispersion for seven regions.

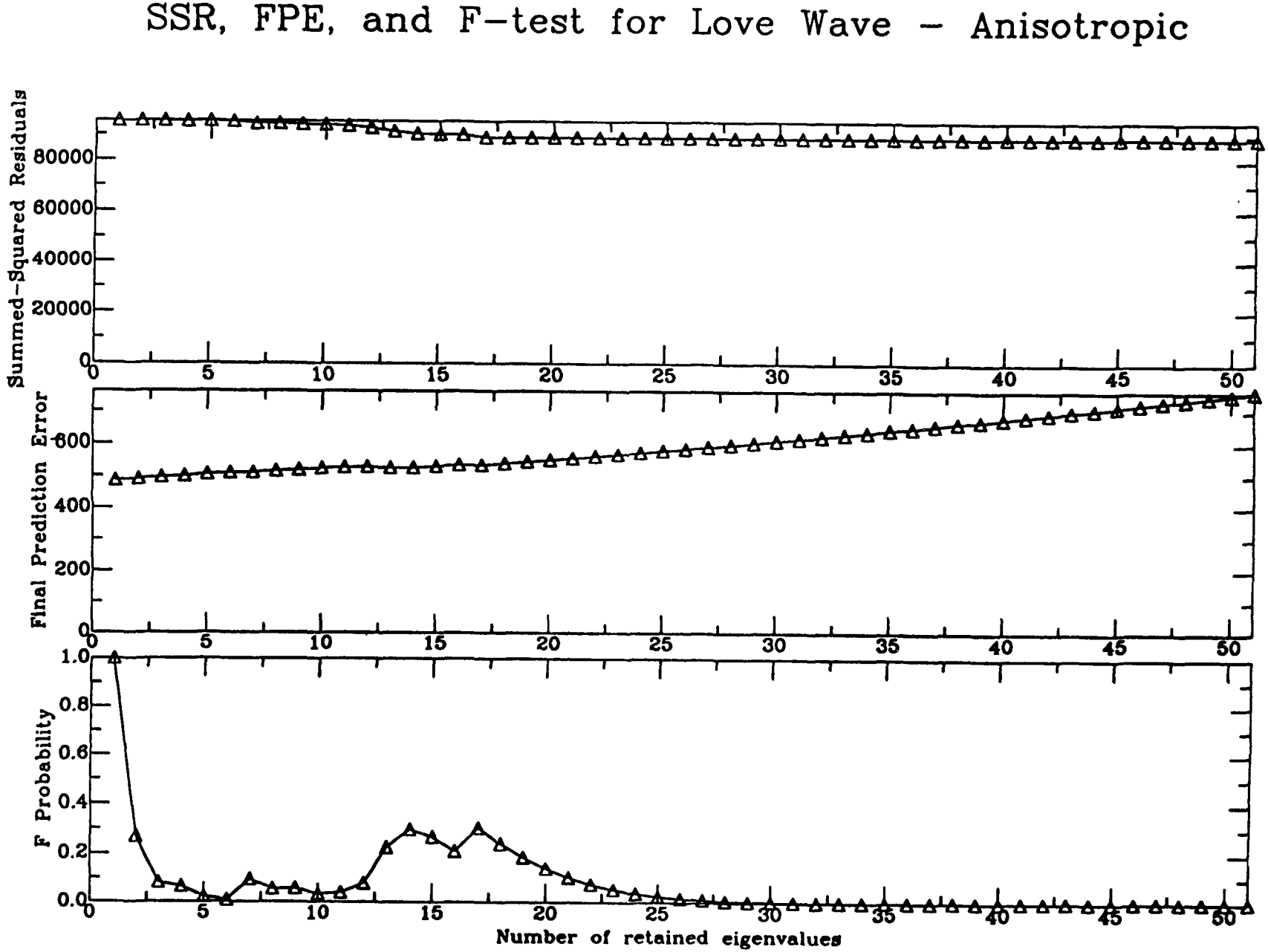

Figure 11. SSR, F-test and FPE values versus number of retained eigenvalues.

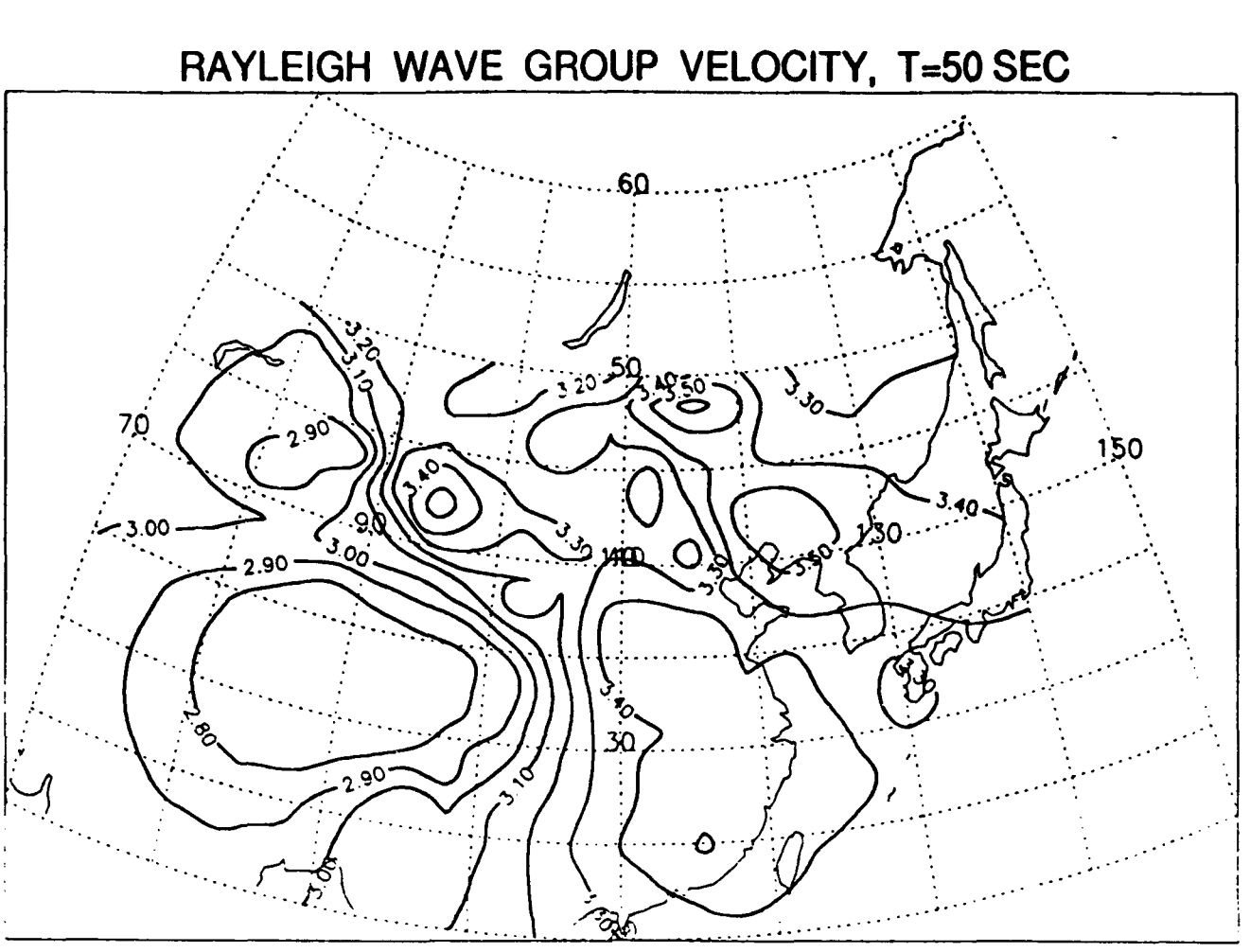

Figure 12. Tomography results for Rayleigh wave group velocity at 50 sec period.

ANALYSIS OF REGIONAL BODYWAVE PHASES FROM EARTHQUAKES IN EASTERN ASIA

Jeffrey S, Barker

State University of New York, Binghamton

OBJECTIVE:

The purpose of this study is to improve our understanding of the crustal waveguide phases, P_g and L_g, by modeling regional waveforms in eastern Asia. Burdick et al. (1989) have demonstrated that deterministic modeling of high-frequency P_n and P_g from NTS explosions can fit waveforms recorded on a regional network and provide valuable information on regional wave propagation characteristics. We wish to apply this sort of approach to regional waveforms from earthquakes and explosions in eastern Asia, making use of the recent high-quality, broad-band data recorded on the Chinese Digital Seismic Network (CDSN). Unfortunately the station spacing is quite sparse, so that for a given event, little correlation between stations may be made. Without independent information on crustal structure, there will remain a certain level of ambiguity in the identification of the arrivals that interfere to generate the P_n-P_g waveform.

In order to minimize this ambiguity, we begin by modeling broad-band P_n and P_g waveforms from profiles of earthquakes recorded at the CDSN station WMQ. This is not really the reciprocal experiment since the earthquakes have different depths, magnitudes and mechanisms. However, Wu (1990) showed that the P waveforms from these earthquakes have many similarities, and we may interpret these in terms of the moveout of specific crustal phases. By simultaneously modeling the waveforms from each of these earthquakes, we gain an understanding not only of regional P-wave propagation near WMQ, but also of the kinds of variations observed in the waveforms for different source depths and mechanisms. By modeling profiles along different azimuths or recorded at different stations, we may investigate the effect of different crustal structures, or the effect of

lateral variations in structure. Finally, we may use this understanding to model high-frequency P_n-P_g waveforms from Kazakh explosions, or individual sources from other locations in eastern Asia.

RESEARCH ACCOMPLISHED:

As a first profile, we consider earthquakes along a line SW of WMQ (Figure 1 and Table 1), from the Tarim Basin and the Tienshan regions of western China. In a surface wave regionalization study (Wu and Jones, "Surface wave regionalization and tomography in China and its vicinity", this report), these are considered to be within the same structural region, so lateral variations in crustal structure should be minimal. With one exception, these are shallow crustal earthquakes (depths 8-33 km) with thrust mechanisms. The exception is an event in the Pamir valley (87276) which occurred at a depth of 80 km. Since it is also our most distant event from WMQ, we will not consider it in the initial modeling, but only later to test the modeling at greater ranges and source depths. Broad-band seismograms from the other events have been processed to facilitate comparison with synthetic seismograms. This processing includes time integration (to ground displacement) and a high-pass Butterworth filter (frequency 0.08 Hz) to reduce low-frequency drift in the synthetics. In this study we are concentrating on the P_n-P_g wavetrain, so only the vertical component is modeled.

A profile of the vertical-component waveforms is shown on the left side of Figure 2. Superimposed on the waveforms are travel-time curves appropriate for various P and S phases for a source at 30 km depth in a layered velocity structure model (discussed below). To facilitate comparison between events, the waveforms in the figure have been band-pass filtered from 0.5 - 2.0 Hz, and time shifts have been applied to three of the records. For events 87005 (560 km) and 87159 (1175 km), a time lead of 2 sec is used, while for event 87351 (422 km) a lag of 3 sec is used. These may reflect errors in the assumed origin time of these events, or simply variations due to source depth. The first 40-50 sec of these waveforms are shown on the left side of Figure 3,

along with travel-time curved for selected phases. A number of features in the observed waveforms correlate with some of these predicted arrivals. In particular, for the closest event, P, pP and S may be identified. Beyond 400 km, P_n and P may be identified, but P_MP is not a substantial arrival. In fact, for these mechanisms, sP_n and sP_MP may be seen as an elongated series of arrivals at 400-600 km and as distinct phases at 1175 km. Many other arrivals are present in the observed waveforms; the travel-time curves show only selected arrivals for a single source depth.

Other features are better modeled by computing synthetic seismograms for the appropriate range, depth and mechanism and comparing this with the observed waveform. The velocity structure model assumed (Table 3, Figure 4) is based on the surface wave results of Feng and Teng (1983), modified so that the travel-time curves provide reasonable agreement to observed arrival times (as in Figure 3). The Moho is at a depth of 56 km, while a mid-crustal discontinuity is located at 41 km depth. In the figures to follow, reflections from the Moho are denoted P_MP, while those from the mid-crustal disctoninuity are denoted P_CP. A velocity gradient is included in the mantle so that P_n is modeled as a turning ray rather than as a head wave. The initial synthetics were computed using generalized ray theory (Helmberger and Harkrider, 1978) in order to identify important phases in the high-frequency P_n-P_g waveform. In all, 75 rays arriving as P waves were allowed, including up to three reverberations in the crust and mode conversions at the free surface and the Moho. More complete synthetics were computed using a frequency-wavenumber (F-K) integration technique (Barker, 1984). This method uses the compound matrix modification of the Haskell layer matrix method with Filon quadrature over wavenumber. Anelastic attenuation is included to move the poles off of the real-k axis. No wavenumber filtering is imposed, so the synthetics include S waves and surface waves in addition to the P wavetrain. These are computation-intensive synthetics, so we must limit the frequency band and time duration (up to 4 Hz, 512 sec duration). The source parameters used in generating the synthetics are listed in Table 2. These include Harvard CMT mechanisms (published in the PDE) when available; otherwise an average mechanism is assumed. Source corner frequencies and Butterworth filter parameters are chosen to give the best agreement

between data and synthetics. Source depths (again from the PDE) are sometimes questionable, so the synthetics are computed at 10, 20 and 30 km depths, and the depth closest to that reported for an event is used in the comparison.

Profiles of F-K synthetics for a source depth of 30 km are shown on the right sides of Figures 2 and 3. Although some wrap-around is apparent at the beginning of the traces, P_g and several later arrivals may be easily identified. The synthetics are somewhat simpler than the observed waveforms (compare the two sides of Figure 3), but many features are common. For example, at 400 km sP_g and sP_MP interfere to generate an elongated wavetrain. Although the travel-time curves are not shown, the second and third P-wave reverberations in the crust also arrive between 20-30 sec (reduced time) at this range. With increasing range, sP_g becomes the dominant phase, interfering with P_MP at 1200 km range. Higher-order crustal multiples (P_MPP_MP, S_MPP_MP, etc.) do not appear to play a dominant role in either the observed or synthetic waveforms for these earthquakes. Certainly the strength of the upgoing S wave that reflects from the free surface is dependent on the radiation pattern, and in this profile we are considering only earthquakes along a single azimuth and with comparable mechanisms. For near-surface isotropic sources (explosions), we would expect crustal multiples to dominate the waveform as Burdick et al. (1989) found for NTS. This is an example of how radiation pattern can cause substantial difference in the generation of the high-frequency P_g-P_g waveform, and may be exploited as a discriminant.

Since the P_g-P_g waveforms result from the interference of a number of phases which depart the source either upward or downward, it is instructive to see how this interference varies with changes in source depth. Shown in Figures 5 - 9 are observed vertical-component waveforms for five of the events in the SW profile, along with F-K synthetics computed for 10, 20 and 30 km source depths. With the exception of event 87279 (Figure 5), the traces have been aligned on the P_g wave (87279 is at pre-citical range, so is aligned on P). Upward departing phases (such as sP_g) move out in time with increasing source depth, while downward departing phases (such as P_MP) remain stationary or move in. The arrival times of important phases, determined from generalized

ray synthetics, are indicated on the figures. At different ranges, different phases interfere to form the arrivals observed on the vertical-component seismogram. For example, for event 87279 (82 km, Figure 5), P_MP is a relatively minor phase, but pP_MP and $(P_CP)_2$ (a double reverberation in the upper crust) interfere at 30 km depth to produce a single large-amplitude arrival, which corresponds to the largest arrival in the observed seismogram. The published depth for this event is 32 km, which is consistent with the depth inferred from the synthetics (denoted by the arrow in Figure 5).

For event 87351 (422 km, Figure 6), crustal phases are well separated, resulting in the elongated series of arrivals observed for this event. If the depth is somewhat greater than 30 km (as indicated), arrivals observed at about 18 sec and 33 sec may be interpreted as sP_n and $s(P_MP)_2$, respectively. The large-amplitude, late arrival in the synthetics is Sn which, as usual, is substantially larger in the synthetics than in the observed waveform. At 560 km (event 87005, Figure 7), none of the computed synthetics matches the arrival times of all of the observed phases, but from the relative moveout of P_n, P and sP_n, we can see that a source depth of 14-15 km would produce an excellent fit. The published depth for this event is 17 km. On the other hand, for event 98024a (731 km, Figure 8), a source depth of about 16 km would provide a better fit (particularly for sP_CP and $s(P_MP)_2$) than the published depth of 30 km. Finally, for event 87159 (1175 km, Figure 9), the published mechanism is clearly inconsistent with the observed P-wave polarities at WMQ. However, since the crustal phases are well separated in time at this range, we interpret that the source must have been shallower than the published depth of 10 km.

CONCLUSIONS AND RECOMMENDATIONS:

For the earthquake profile SW of WMQ, broad-band P_n-P_g waveforms can be well modeled, and appear to be dominated by S waves that depart the source upward, then reflect and convert to P waves at the free surface (e.g. sP_n). Since this conclusion is radiation-pattern dependent, we would expect other phases to dominate for other mechanisms or other azimuths. Nevertheless, once phases are identified through synthetic modeling, depth-dependent variations in waveforms due to the

interference of these phases can contribute toward discrimination. With an improved understanding of the phases that interfere to generate the crustal waveguide phases, if becomes increasingly possible to model with confidence the P_n-P_g wavetrains observed at sparsely distributed stations. What we learn about wave propagation in western China is applicable to regional discrimination in any part of the world.

REFERENCES:

Barker, J.S. (1984). A seismological analysis of the 1980 Mammoth Lakes, California, earthquakes, *PhD Thesis*, Pennsylvania State Univ.

Bennett, T.J., J.F. Scheimer, A.K. Campanella and J.R. Murphy (1990). Regional discrimination research and methodology implementation: Analyses of CDSN and Soviet IRIS data, *Scientific Report No. 4, GL-TR-90-0194*, Air Force Geophysics Laboratory, ADA230251.

Burdick, L.J., C.K. Saikia and D.V. Helmberger (1989). Deterministic modeling of regional waveforms from the Nevada Test Site, *Final Report. GL-TR-89-0196*, Air Force Geophysics Laboratory, ADA216641.

Feng, C.C. and T.L. Teng (1983). Three dimensional crust and upper mantle structure of the Eurasian continent, *J. Geophys. Res.*, *88*, 2261-2272.

Helmberger, D.V. and D.G. Harkrider (1978). Modeling earthquakes with generalized ray theory, in *Proc. IUTAM Symp.: Modern Problems in Elastic Wave Propagation*, J. Miklowitz and J. Achenback, eds., Wiley.

Wu, F.T. (1990). Studies of regional phases and discriminants in Asia, *Final Report, GL-TR-90-0017*, Air Force Geophysics Laboratory, ADA222184.

Table 1 - Earthquakes along the SW Profile from WMQ

Date	Time (GMT)	Lat. (°N)	Lon (°E)	R (km)	Az (°)	Depth (km)	m_b
10/6/87 (87279)	1306:20.3	43.44	88.55	82.0	302	32	4.8
12/17/87 (87351)	1217:25.0	41.94	83.20	421.9	59	33	5.1
8/5/87 (87217)	1024:21.0	41.36	82.11	534.1	57	33	4.8
1/5/87 (87005)	2252:46.5	41.96	81.32	559.6	66	17	5.9
1/24/87 (87024a)	0809:21.0	41.53	79.32	731.2	67	29	5.9
1/24/87 (87024b)	1340:40.0	41.44	79.25	740.5	66	33	5.2
6/8/87 (87159)	1330:36.0	39.79	74.69	1175.0	63	10	5.1
4/30/87 (87120)	0517:37.0	39.76	74.57	1178.3	63	8	5.7
10/3/87 (87276)	1100:03.3	36.45	71.44	1604.3	54	80	6.0

Compiled from PDE, Wu (1990), and Bennett et al. (1990).

Table 2 - Parameters Used in Generating the Synthetics

	Mechanism and Corner Frequency				Highpass[c]		Lowpass[c]	
Date	Strike[a] (°)	Dip[a] (°)	Rake[a] (°)	fc (Hz)	poles	f (Hz)	poles	f (Hz)
87279	220[b]	40[b]	65[b]	>4	3	0.2		
87351	220[b]	40[b]	65[b]	0.5	3	0.3	1	1.5
87005	226	21	47	0.8	3	0.05		
87024a	268	45	107	0.8	3	0.03	3	1.0
87159	298	27	91	0.3	1	0.08	3	2.0

[a] Mechanisms are Harvard CMT solutions published in the PDE.
[b] No mechanism published. These vales are assumed.
[c] Butterworth one-pass (causal) filters.

Table 3 - Structure Model for SW Profile Synthetics

V_P (km/s)	V_S (km/s)	Density (g/cm^3)	Thickness (km)	Q_P	Q_S
4.80	2.77	2.58	9.0	300	150
6.25	3.61	2.79	32.0	800	400
7.25	4.18	3.00	15.0	1000	500
8.00	4.62	3.33	20.0	1200	600
8.10	4.68	3.36	20.0	1200	600
8.20	4.73	3.40	40.0	1200	600
8.30	4.79	3.45	-	1200	600

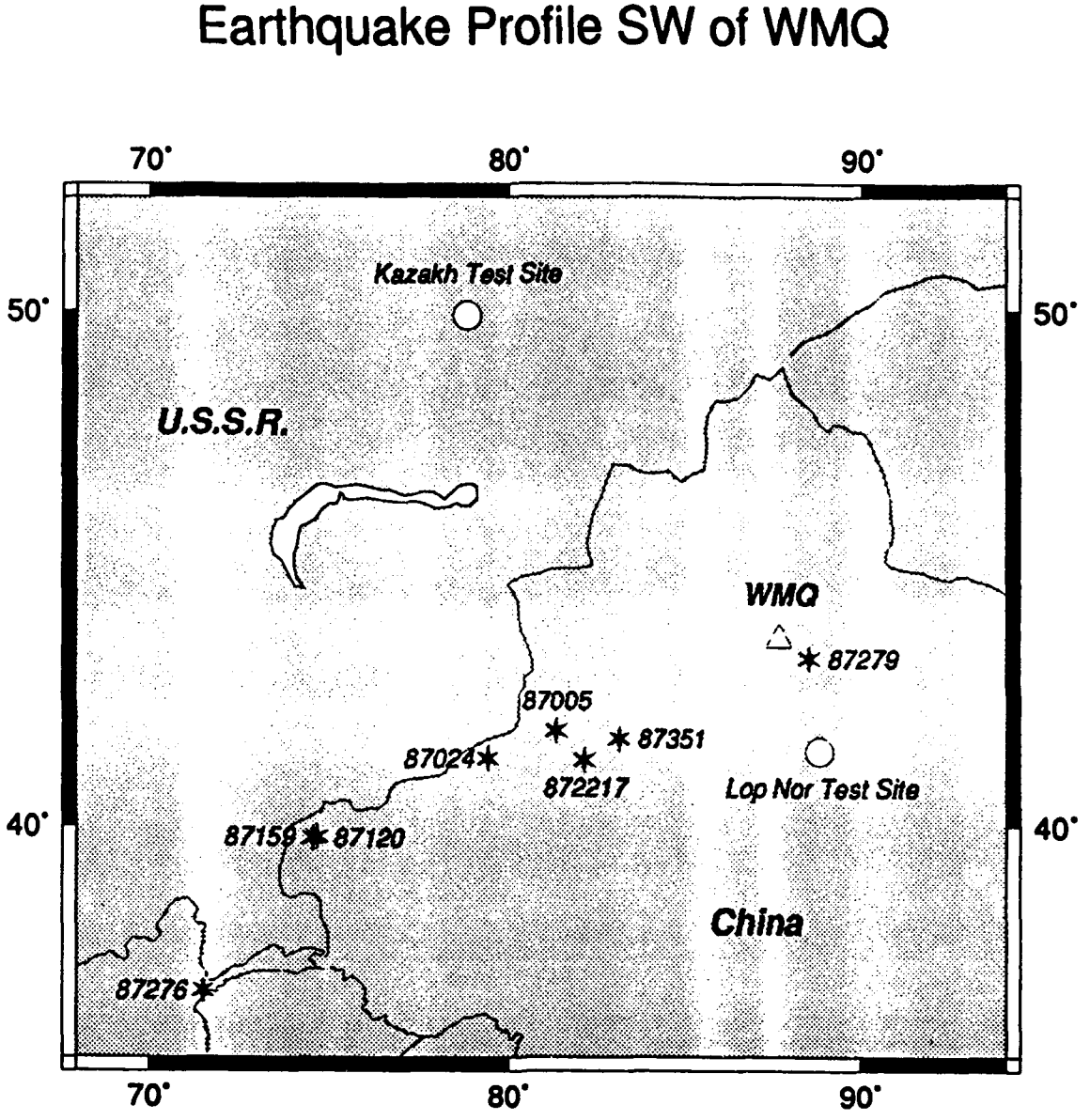

Fig. 1 Map of northwestern China showing the locations of earthquakes located along a profile SW of CDSN station WMQ. Also shown are the locations of the Kazakh test site and the Lop Nor test site.

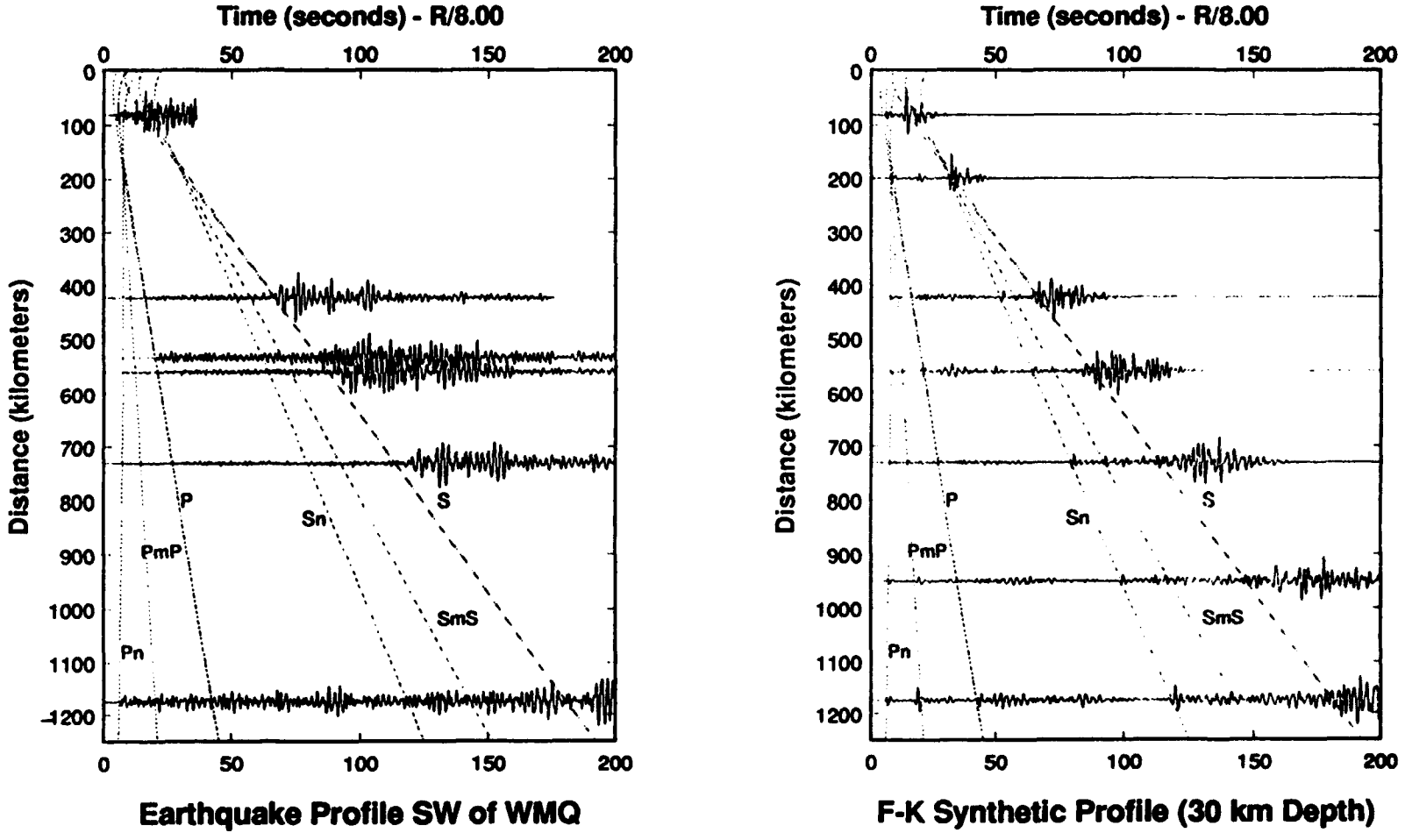

Fig. 2 (left) A profile of P_n-P_g waveforms from earthquakes to the SW recorded at WMQ, plotted with a reduction velocity of 8 km/s. Also shown are travel-time curves for important P- and S-wave phases computed for a source at 30 km depth in the velocity structure model in Table 3. Since the observed waveforms are from earthquakes at different depths, some waveforms have been time shifted slightly. (right) A profile of F-K synthetic seismograms for a sources at a depth of 30 km located SW of WMQ. Superimposed are the same travel-time curves as plotted on the observed data profile.

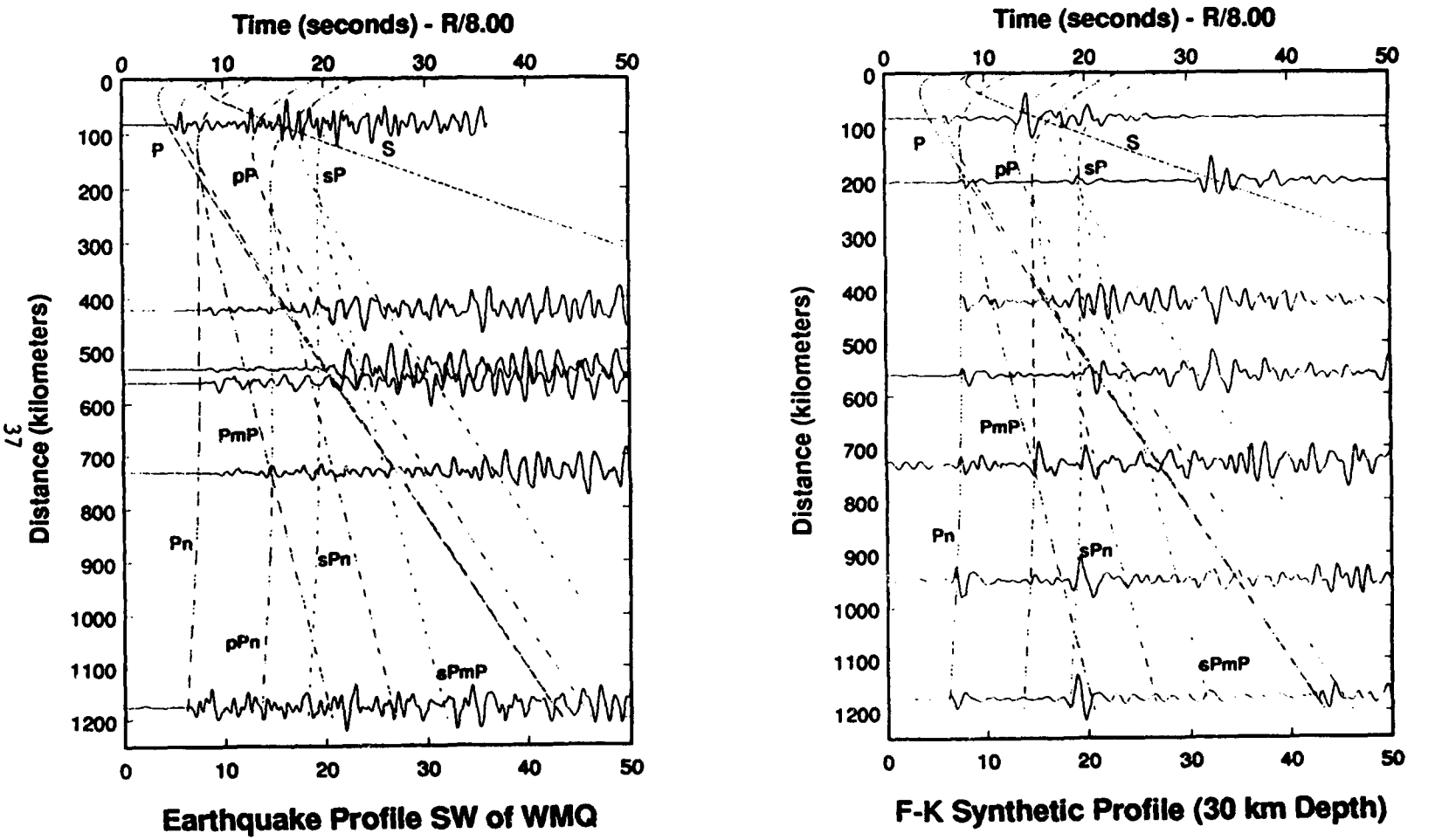

Fig. 3 (left) The same profile of observed waveforms as in Figure 2, but now limited to the P_n-P_g time window (the first 40-50 sec). Travel-time curves for important phases computed for a source depth of 30 km are shown. (right) The profile of F-K synthetics for the P_n-P_g portion of the waveforms.

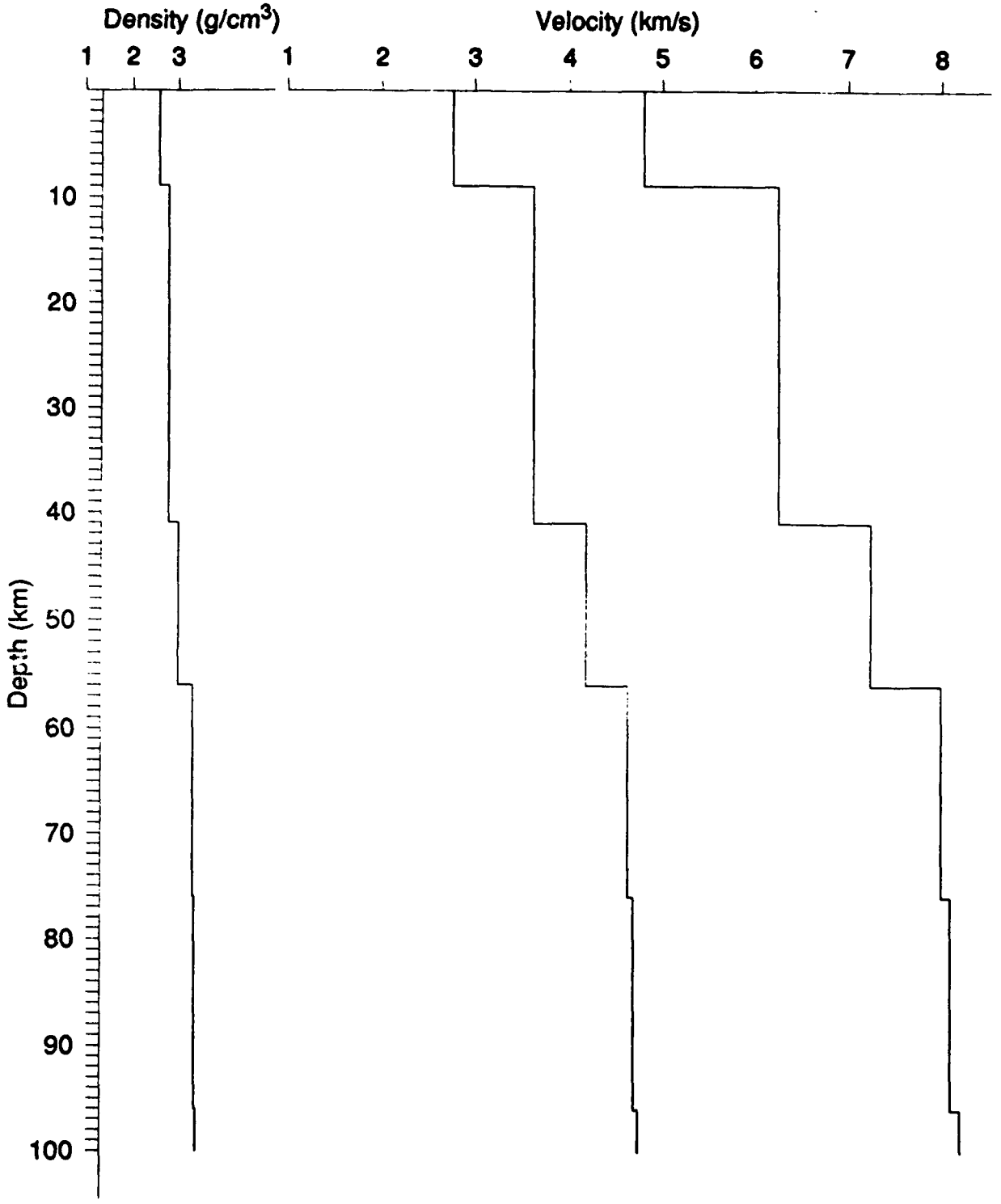

Fig. 4 The velocity and density structure model assumed in computing travel-time curves and synthetic seismograms. The model is derived from the surface-wave results of Feng and Teng (1983), modified so that travel-time curves provide reasonable agreement with observed arrival times.

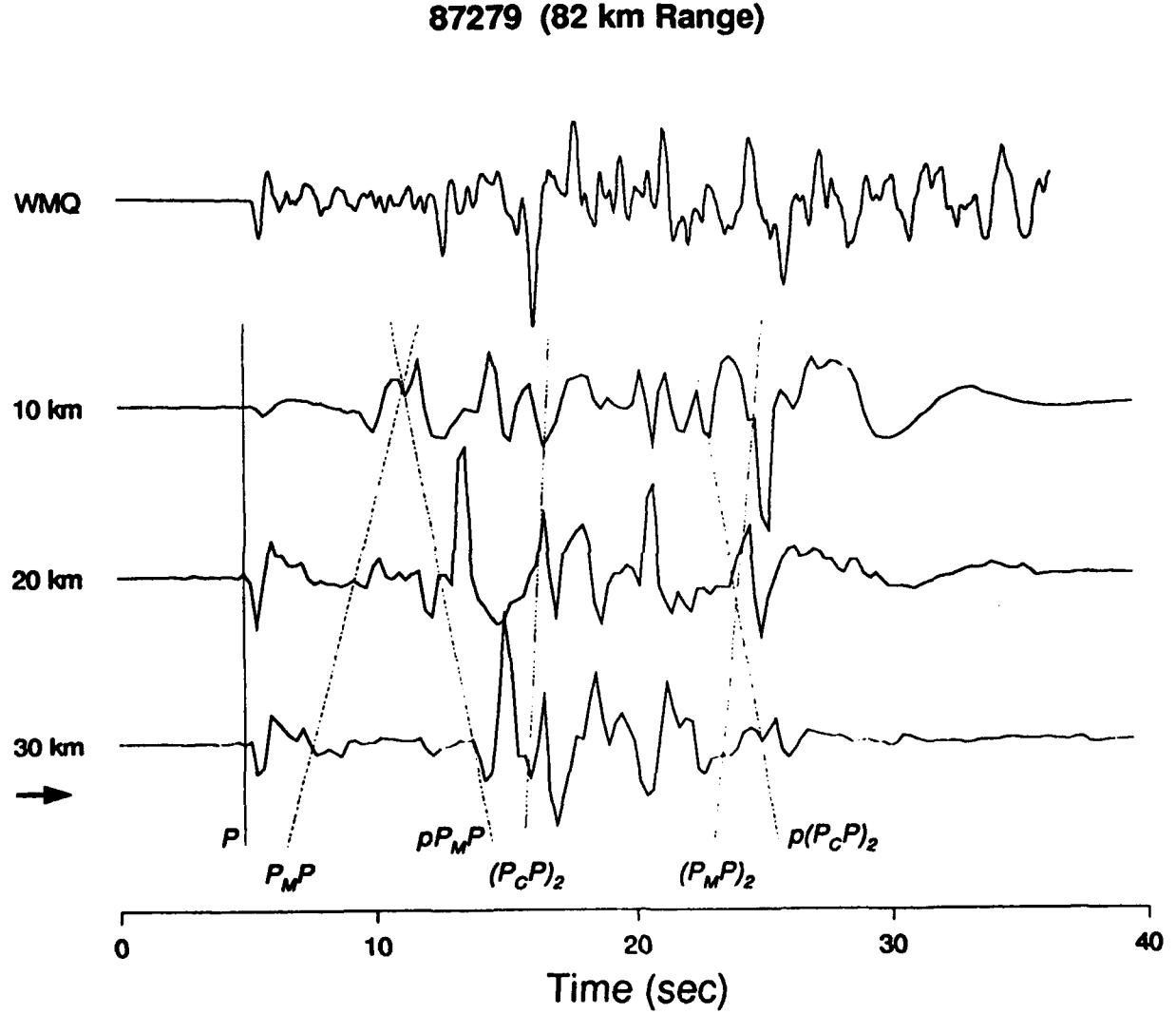

Fig. 5 A comparison of the observed P_n-P_g waveform (top trace) from event 87279 (82 km range) at WMQ with F-K synthetics (lower traces) computed for source depths of 10, 20 and 30 km. The traces are aligned on the P wave. Arrival times of significant phases, determined by generalized ray theory, are indicated on the synthetics. The variations in moveout for upgoing and downgoing phases changes the interference of arrivals, enabling the interpretation of source depth as slightly greater than 30 km (denoted by the arrow).

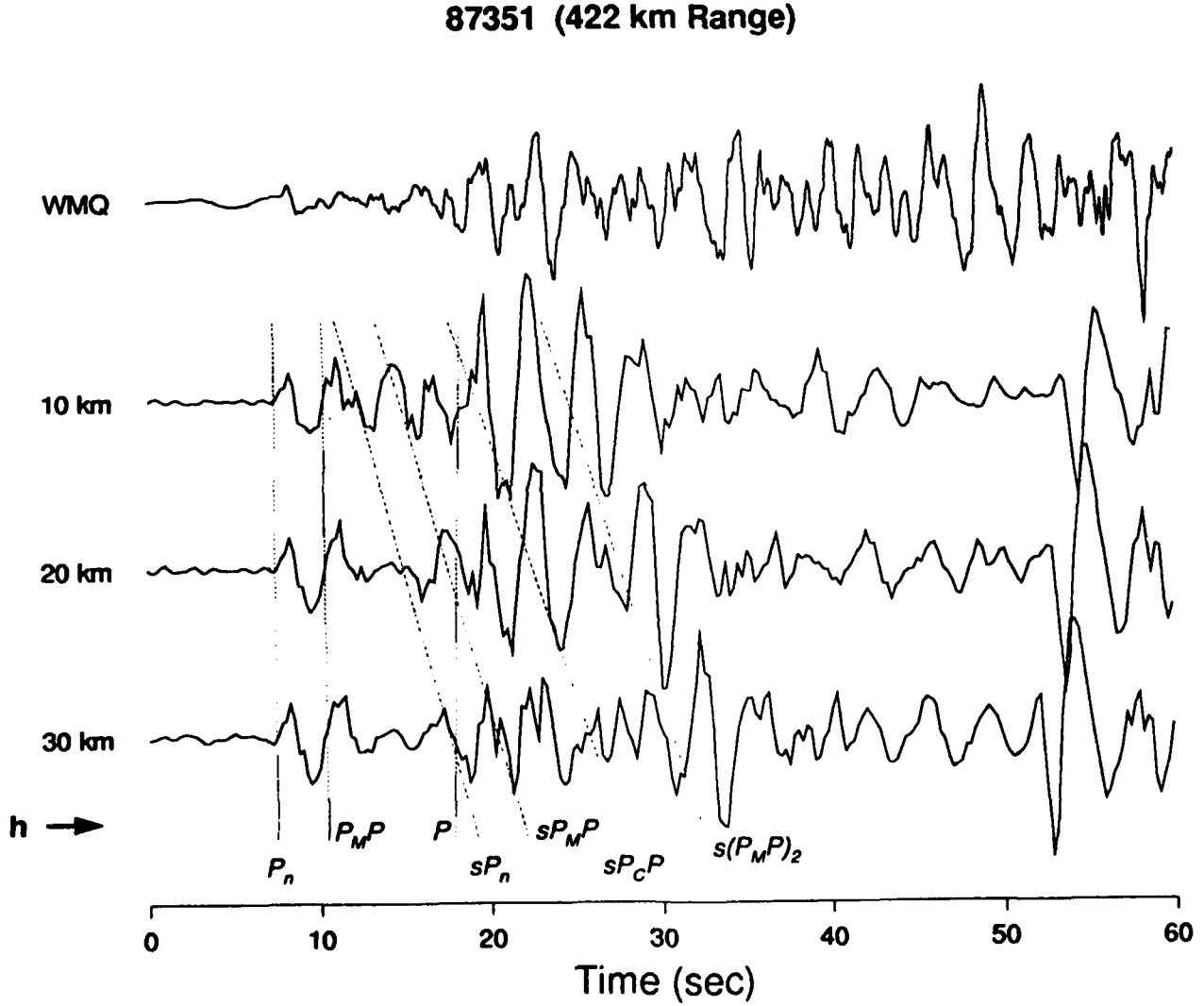

Fig. 6 A comparison of observed and synthetic P_n-P_g waveforms from event 87351 (442 km range) at WMQ. The format is the same as Figure 5, except that the traces are now aligned on P_n. The interference of arrivals causes an elongated P_n-P_g wavetrain. Arrivals corresponding to sP_n and $s(P_MP)_2$ are best fit for a source depth greater than 30 km.

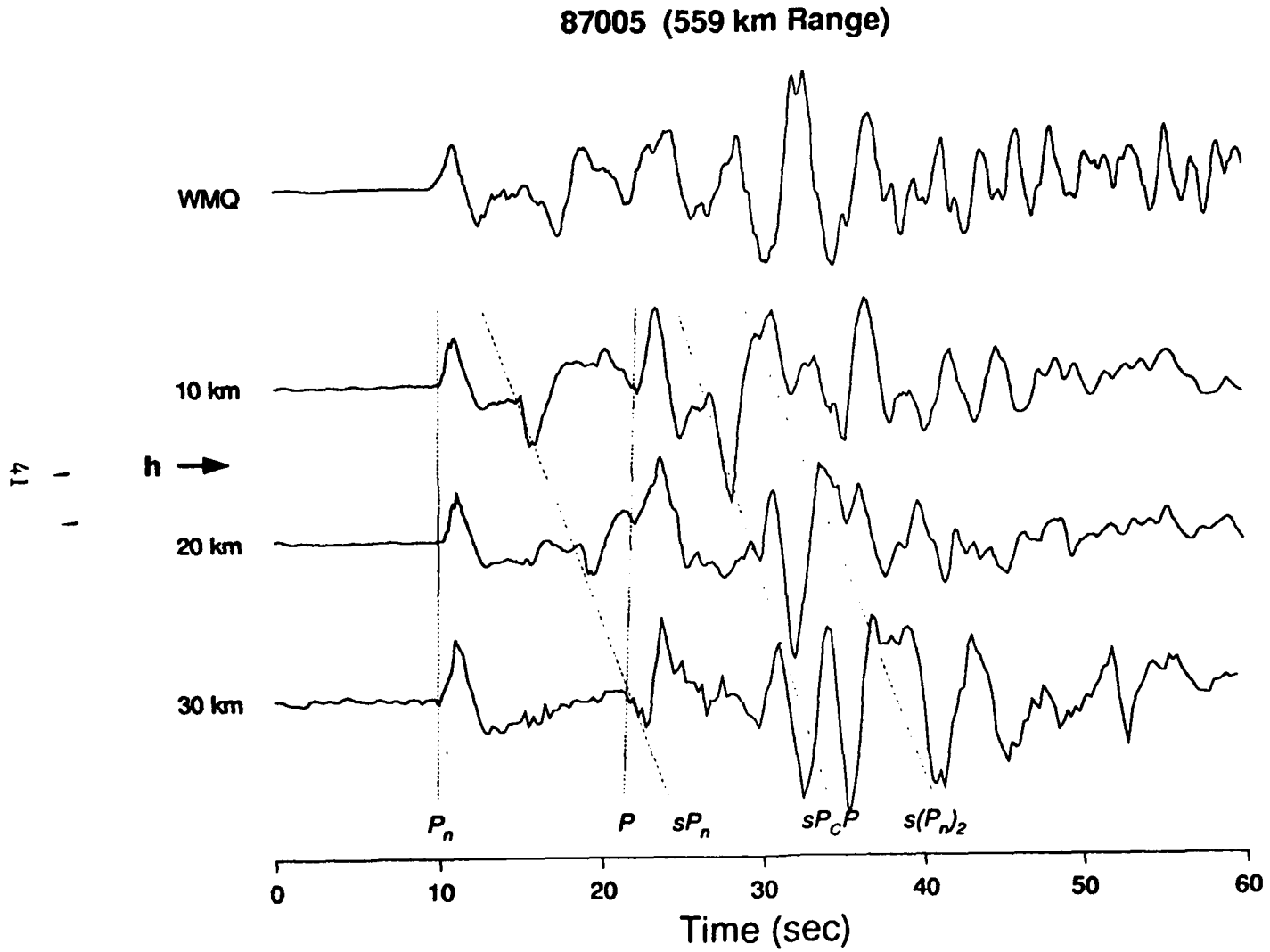

Fig. 7 A comparison of observed and synthetic P_n-P_g waveforms from event 87005 (559 km range) at WMQ. The format is the same as Figure 6. In this case, the relative arrival times of sP_CP and $s(P_n)_2$ suggest a source depth of 14-15 km.

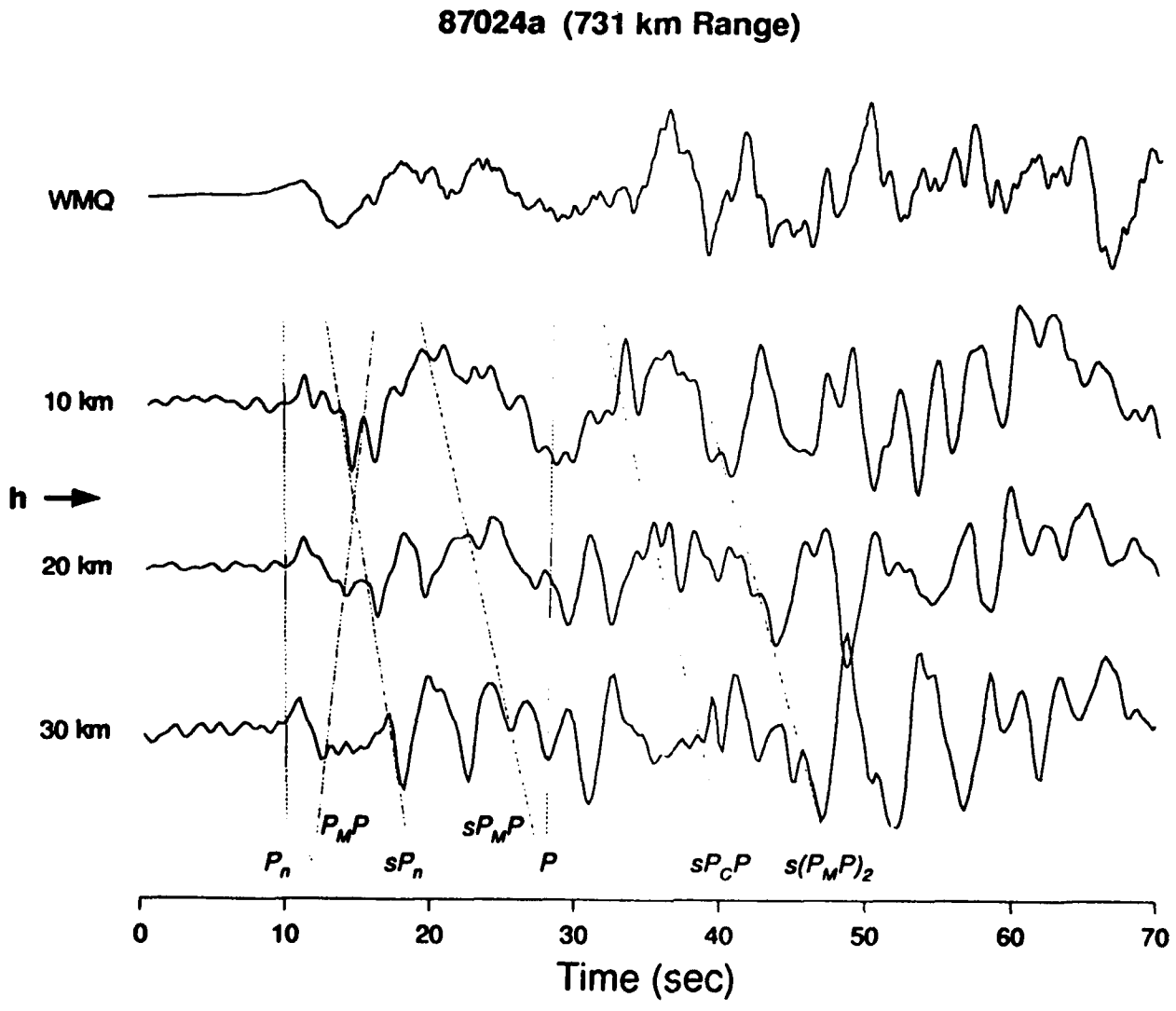

Fig. 8 A comparison of observed and synthetic P_n-P_g waveforms from event 87024a (731 km range) at WMQ. The format is the same as Figure 6. The source depth, based on largely on sP_CP and $s(P_MP)_2$ arrival times, is about 16 km.

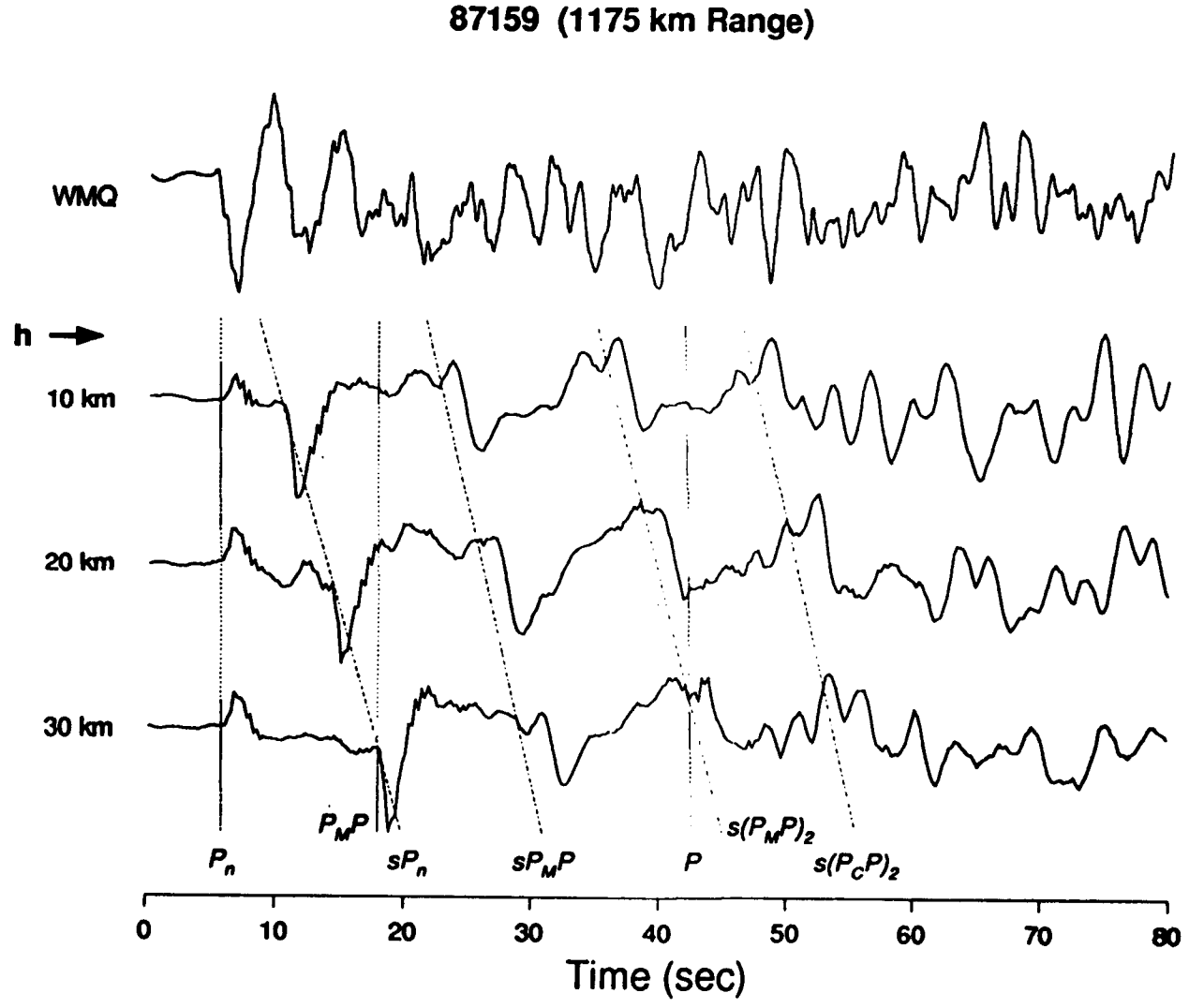

Fig. 9 A comparison of observed and synthetic P_n-P_g waveforms from event 87159 (1175 km range) at WMQ. The format is the same as Figure 6. The published mechanism results in incorrect P-wave polarities at WMQ. However, based on arrival times, we interpret the source depth as less than 10 km.

DISTRIBUTION LIST

Prof. Thomas Ahrens
Seismological Lab, 252-21
Division of Geological & Planetary Sciences
California Institute of Technology
Pasadena, CA 91125

Prof. Keiiti Aki
Center for Earth Sciences
University of Southern California
University Park
Los Angeles, CA 90089-0741

Prof. Shelton Alexander
Geosciences Department
403 Deike Building
The Pennsylvania State University
University Park, PA 16802

Dr. Ralph Alewine, III
DARPA/NMRO
3701 North Fa[illegible] Drive
Arlington, V[illegible] 03-1714

Prof. Charles B. Archambeau
CIRES
University of Colorado
Boulder, CO 80309

Dr. Thomas C. Bache, Jr.
Science Applications Int'l Corp.
10260 Campus Point Drive
San Diego, CA 92121 (2 copies)

Prof. Muawia Barazangi
Institute for the Study of the Continent
Cornell University
Ithaca, NY 14853

Dr. Jeff Barker
Department of Geological Sciences
State University of New York
at Binghamton
Vestal, NY 13901

Dr. Douglas R. Baumgardt
ENSCO, Inc
5400 Port Royal Road
Springfield, VA 22151-2388

Dr. Susan Beck
Department of Geosciences
Building #77
University of Arizona
Tuscon, AZ 85721

Dr. T.J. Bennett
S-CUBED
A Division of Maxwell Laboratories
11800 Sunrise Valley Drive, Suite 1212
Reston, VA 22091

Dr. Robert Blandford
AFTAC/TT, Center for Seismic Studies
1300 North 17th Street
Suite 1450
Arlington, VA 22209-2308

Dr. G.A. Bollinger
Department of Geological Sciences
Virginia Polytechnical Institute
21044 Derring Hall
Blacksburg, VA 24061

Dr. Stephen Bratt
Center for Seismic Studies
1300 North 17th Street
Suite 1450
Arlington, VA 22209-2308

Dr. Lawrence Burdick
Woodward-Clyde Consultants
566 El Dorado Street
Pasadena, CA 91109-3245

Dr. Robert Burridge
Schlumberger-Doll Research Center
Old Quarry Road
Ridgefield, CT 06877

Dr. Jerry Carter
Center for Seismic Studies
1300 North 17th Street
Suite 1450
Arlington, VA 22209-2308

Dr. Eric Chael
Division [redacted] MS-0655
Sandia Laboratory
Albuquerque, NM 87185-0655

Prof. Vernon F. Cormier
Department of Geology & Geophysics
U-45, Room 207
University of Connecticut
Storrs, CT 06268

Prof. Steven Day
Department of Geological Sciences
San Diego State University
San Diego, CA 92182

US Dept of Energy
Recipient, IS-20, GA-033
Office of Rsch & Development
100 Independence Ave, SW
Washington, DC 20585

Dr. Zoltan Der
ENSCO, Inc.
5400 Port Royal Road
Springfield, VA 22151-2388

Prof. Adam Dziewonski
Hoffman Laboratory, Harvard University
Dept. of Earth Atmos. & Planetary Sciences
20 Oxford Street
Cambridge, MA 02138

Prof. John Ebel
Department of Geology & Geophysics
Boston College
Chestnut Hill, MA 02167

Eric Fielding
SNEE Hall
INSTOC
Cornell University
Ithaca, NY 14853

Dr. Mark D. Fisk
Mission Research Corporation
735 State Street
P.O. Drawer 719
Santa Barbara, CA 93102

Prof Stanley Flatte
Applied Sciences Building
University of California, Santa Cruz
Santa Cruz, CA 95064

Prof. Donald Forsyth
Department of Geological Sciences
Brown University
Providence, RI 02912

Dr. Art Frankel
U.S. Geological Survey
922 National Center
Reston, VA 22092

Dr. Cliff Frolich
Institute of Geophysics
8701 North Mopac
Austin, TX 78759

Dr. Holly Given
IGPP, A-025
Scripps Institute of Oceanography
University of California, San Diego
La Jolla, CA 92093

Dr. Jeffrey W. Given
SAIC
10260 Campus Point Drive
San Diego, CA 92121

Dr. Dale Glover
Defense Intelligence Agency
ATTN: ODT-1B
Washington, DC 20301

Dr. Indra Gupta
Teledyne Geotech
1300 17th Street N, #1450
Arlington, VA 22209-3803

Dan N. Hagedon
Pacific Northwest Laboratories
Battelle Boulevard
Richland, WA 99352

Dr. James Hannon
Lawrence Livermore National Laboratory
P.O. Box 808
L-205
Livermore, CA 94550

Dr. Roger Hansen
HQ AFTAC/TTR
Patrick AFB, FL 32925-6001

Prof. David G. Harkrider
Seismological Laboratory
Division of Geological & Planetary Sciences
California Institute of Technology
Pasadena, CA 91125

Prof. Danny Harvey
CIRES
University of Colorado
Boulder, CO 80309

Prof. Donald V. Helmberger
Seismological Laboratory
Division of Geological & Planetary Sciences
California Institute of Technology
Pasadena, CA 91125

Prof. Eugene Herrin
Institute for the Study of Earth and Man
Geophysical Laboratory
Southern Methodist University
Dallas, TX 75275

Prof. Robert B. Herrmann
Department of Earth & Atmospheric Sciences
St. Louis University
St. Louis, MO 63156

Prof. Lane R. Johnson
Seismographic Station
University of California
Berkeley, CA 94720

Prof. Thomas H. Jordan
Department of Earth, Atmospheric &
Planetary Sciences
Massachusetts Institute of Technology
Cambridge, MA 02139

Prof. Alan Kafka
Department of Geology & Geophysics
Boston College
Chestnut Hill, MA 02167

Robert C. Kemerait
ENSCO, Inc.
445 Pineda Court
Melbourne, FL 32940

US Dept of Energy
Attn: Max Koontz, NN-20, GA-033
Office of Rsch & Development
1000 Independence Ave, SW
Washington, DC 20585

Dr. Richard LaCoss
MIT Lincoln Laboratory, M-200B
P.O. Box 73
Lexington, MA 02173-0073

Dr. Fred K. Lamb
University of Illinois at Urbana-Champaign
Department of Physics
1110 West Green Street
Urbana, IL 61801

Prof. Charles A. Langston
Geosciences Department
403 Deike Building
The Pennsylvania State University
University Park, PA 16802

Jim Lawson, Chief Geophysicist
Oklahoma Geological Survey
Oklahoma Geophysical Observatory
P.O. Box 8
Leonard, OK 74043-0008

Prof. Thorne Lay
Institute of Tectonics
Earth Science Board
University of California, Santa Cruz
Santa Cruz, CA 95064

Dr. William Leith
U.S. Geological Survey
Mail Stop 928
Reston, VA 22092

Mr. James F. Lewkowicz
Phillips Laboratory/GPEH
Hanscom AFB, MA 01731-5000(2 copies)

Mr. Alfred Lieberman
ACDA/VI-OA State Department Building
Room 5726
320-21st Street, NW
Washington, DC 20451

Prof. L. Timothy Long
School of Geophysical Sciences
Georgia Institute of Technology
Atlanta, GA 30332

Dr. Randolph Martin, III
New England Research, Inc.
76 Olcott Drive
White River Junction, VT 05001

Dr. Robert Masse
Denver Federal Building
Box 25046, Mail Stop 967
Denver, CO 80225

Dr. Gary McCartor
Department of Physics
Southern Methodist University
Dallas, TX 75275

Prof. Thomas V. McEvilly
Seismographic Station
University of California
Berkeley, CA 94720

Dr. Art McGarr
U.S. Geological Survey
Mail Stop 977
U.S. Geological Survey
Menlo Park, CA 94025

Dr. Keith L. McLaughlin
S-CUBED
A Division of Maxwell Laboratory
P.O. Box 1620
La Jolla, CA 92038-1620

Stephen Miller & Dr. Alexander Florence
SRI International
333 Ravenswood Avenue
Box AF 116
Menlo Park, CA 94025-3493

Prof. Bernard Minster
IGPP, A-025
Scripps Institute of Oceanography
University of California, San Diego
La Jolla, CA 92093

Prof. Brian J. Mitchell
Department of Earth & Atmospheric Sciences
St. Louis University
St. Louis, MO 63156

Mr. Jack Murphy
S-CUBED
A Division of Maxwell Laboratory
11800 Sunrise Valley Drive, Suite 1212
Reston, VA 22091 (2 Copies)

Dr. Keith K. Nakanishi
Lawrence Livermore National Laboratory
L-025
P.O. Box 808
Livermore, CA 94550

Dr. Carl Newton
Los Alamos National Laboratory
P.O. Box 1663
Mail Stop C335, Group ESS-3
Los Alamos, NM 87545

Dr. Bao Nguyen
HQ AFTAC/TTR
Patrick AFB, FL 32925-6001

Prof. John A. Orcutt
IGPP, A-025
Scripps Institute of Oceanography
University of California, San Diego
La Jolla, CA 92093

Prof. Jeffrey Park
Kline Geology Laboratory
P.O. Box 6666
New Haven, CT 06511-8130

Dr. Howard Patton
Lawrence Livermore National Laboratory
L-025
P.O. Box 808
Livermore, CA 94550

Dr. Frank Pilotte
HQ AFTAC/TT
Patrick AFB, FL 32925-6001

Dr. Robert Reinke
ATTN: FCTVTD
Field Command
Defense Nuclear Agency
Kirtland AFB, NM 87115

Prof. Paul G. Richards
Lamont-Doherty Geological Observatory
of Columbia University
Palisades, NY 10964

Mr. Wilmer Rivers
Teledyne Geotech
314 Montgomery Street
Alexandria, VA 22314

Dr. George Rothe
HQ AFTAC/TTR
Patrick AFB, FL 32925-6001

Dr. Alan S. Ryall, Jr.
DARPA/NMRO
3701 North Fairfax Drive
Arlington, VA 22209-1714

Dr. Richard Sailor
TASC, Inc.
55 Walkers Brook Drive
Reading, MA 01867

Prof. Charles G. Sammis
Center for Earth Sciences
University of Southern California
University Park
Los Angeles, CA 90089-0741

Prof. Christopher H. Scholz
Lamont-Doherty Geological Observatory
of Columbia University
Palisades, CA 10964

Dr. Susan Schwartz
Institute of Tectonics
1156 High Street
Santa Cruz, CA 95064

Secretary of the Air Force
(SAFRD)
Washington, DC 20330

Office of the Secretary of Defense
DDR&E
Washington, DC 20330

Thomas J. Sereno, Jr.
Science Application Int'l Corp.
10260 Campus Point Drive
San Diego, CA 92121

Dr. Michael Shore
Defense Nuclear Agency/SPSS
6801 Telegraph Road
Alexandria, VA 22310

Dr. Matthew Sibol
Virginia Tech
Seismological Observatory
4044 Derring Hall
Blacksburg, VA 24061-0420

Prof. David G. Simpson
IRIS, Inc.
1616 North Fort Myer Drive
Suite 1440
Arlington, VA 22209

Donald L. Springer
Lawrence Livermore National Laboratory
L-025
P.O. Box 808
Livermore, CA 94550

Dr. Jeffrey Stevens
S-CUBED
A Division of Maxwell Laboratory
P.O. Box 1620
La Jolla, CA 92038-1620

Lt. Col. Jim Stobie
ATTN: AFOSR/NL
Bolling AFB
Washington, DC 20332-6448

Brian Stump
Los Alamos National Laboratory
EES-3, Mail Stop C335
Los Alamos, NM 87545

Prof. Jeremiah Sullivan
University of Illinois at Urbana-Champaign
Department of Physics
1110 West Green Street
Urbana, IL 61801

Prof. L. Sykes
Lamont-Doherty Geological Observatory
of Columbia University
Palisades, NY 10964

Dr. David Taylor
ENSCO, Inc.
445 Pineda Court
Melbourne, FL 32940

Dr. Steven R. Taylor
Los Alamos National Laboratory
P.O. Box 1663
Mail Stop C335
Los Alamos, NM 87545

Prof. Clifford Thurber
University of Wisconsin-Madison
Department of Geology & Geophysics
1215 West Dayton Street
Madison, WS 53706

Prof. M. Nafi Toksoz
Earth Resources Lab
Massachusetts Institute of Technology
42 Carleton Street
Cambridge, MA 02142

Dr. Larry Turnbull
CIA-OSWR/NED
Washington, DC 20505

Dr. Gregory van der Vink
IRIS, Inc.
1616 North Fort Myer Drive
Suite 1440
Arlington, VA 22209

Dr. Karl Veith
EG&G
5211 Auth Road
Suite 240
Suitland, MD 20746

Prof. Terry C. Wallace
Department of Geosciences
Building #77
University of Arizona
Tuscon, AZ 85721

Dr. Thomas Weaver
Los Alamos National Laboratory
P.O. Box 1663
Mail Stop C335
Los Alamos, NM 87545

Dr. William Wortman
Mission Research Corporation
8560 Cinderbed Road
Suite 700
Newington, VA 22122

Prof. Francis T. Wu
Department of Geological Sciences
State University of New York
at Binghamton
Vestal, NY 13901

AFTAC/CA
(STINFO)
Patrick AFB, FL 32925-6001

ARPA, OASB/Library
3701 North Fairfax Drive
Arlington, VA 22203-1714

HQ DNA
ATTN: Technical Library
Washington, DC 20305

Defense Intelligence Agency
Directorate for Scientific & Technical Intelligence
ATTN: DTIB
Washington, DC 20340-6158

Defense Technical Information Center
Cameron Station
Alexandria, VA 22314 (2 Copies)

TACTEC
Battelle Memorial Institute
505 King Avenue
Columbus, OH 43201 (Final Report)

Phillips Laboratory
ATTN: XPG
Hanscom AFB, MA 01731-5000

Phillips Laboratory
ATTN: GPE
Hanscom AFB, MA 01731-5000

Phillips Laboratory/TL
Research Library
5 Wright Street
Hanscom AFB, MA 01731-3004

Phillips Laboratory/SUL
3550 Aberdeen Ave, SE
Kirtland AFB, NM 87117-5776 (2 copies)

Dr. Michel Bouchon
I.R.I.G.M.-B.P. 68
38402 St. Martin D'Heres
Cedex, FRANCE

Dr. Michel Campillo
Observatoire de Grenoble
I.R.I.G.M.-B.P. 53
38041 Grenoble, FRANCE

Dr. Kin Yip Chun
Geophysics Division
Physics Department
University of Toronto
Ontario, CANADA

Prof. Hans-Peter Harjes
Institute for Geophysic
Ruhr University/Bochum
P.O. Box 102148
4630 Bochum 1, GERMANY

Prof. Eystein Husebye
NTNF/NORSAR
P.O. Box 51
N-2007 Kjeller, NORWAY

David Jepsen
Acting Head, Nuclear Monitoring Section
Bureau of Mineral Resources
Geology and Geophysics
G.P.O. Box 378, Canberra, AUSTRALIA

Ms. Eva Johannisson
Senior Research Officer
National Defense Research Inst.
P.O. Box 27322
S-102 54 Stockholm, SWEDEN

Dr. Peter Marshall
Procurement Executive
Ministry of Defense
Blacknest, Brimpton
Reading FG7-FRS, UNITED KINGDOM

Dr. Bernard Massinon, Dr. Pierre Mechler
Societe Radiomana
27 rue Claude Bernard
75005 Paris, FRANCE (2 Copies)

Dr. Svein Mykkeltveit
NTNT/NORSAR
P.O. Box 51
N-2007 Kjeller, NORWAY (3 Copies)

Prof. Keith Priestley
University of Cambridge
Bullard Labs, Dept. of Earth Sciences
Madingley Rise, Madingley Road
Cambridge CB3 OEZ, ENGLAND

Dr. Jorg Schlittenhardt
Federal Institute for Geosciences & Nat'l Res.
Postfach 510153
D-[redacted] Hannover [redacted], GERMANY
3c631

Dr. Johannes Schweitzer
Institute of Geophysics
Ruhr University/Bochum
P.O. Box 1102148
4360 Bochum 1, GERMANY